Construction and Building Materials 340 (2022) 127763

Contents lists available at ScienceDirect

Construction and Building Materials

journal homepage: www.elsevier.com/locate/conbuildmat

Short-term and long-term behavior of RC beams strengthened by galvanized steel mesh laminate

Rui Hao [a], Weiwei Lin [a,*], Nasser A. Al-Nuaimi [b,d], Rami A. Hawileh [c], Jamal A. Abdalla [c], Mohammed Z.E.B. Elshafie [d,*]

[a] Department of Civil Engineering, Aalto University, Espoo 02150, Finland
[b] Centre for Advanced Materials, Qatar University, P.O. Box 2713, Doha, Qatar
[c] College of Engineering, American University of Sharjah, United Arab Emirates
[d] College of Engineering, Qatar University, P.O. Box 2713, Doha, Qatar

ARTICLE INFO

Keywords:
Reinforced concrete
Galvanized steel mesh
Interfacial behavior
Numerical simulation

ABSTRACT

Steel reinforced polymers (SRP) are useful in a wide range of applications, including strengthening of existing reinforced concrete (RC) structures, due to their numerous advantages like high strength, low maintenance, light weight and low cost. As such, galvanized steel mesh (GSM) has emerged as an option in the strengthening of RC structures. Although numerous studies were performed on GSM strengthened RC beams, the durability of such strengthening systems is yet to be fully understood. This paper presents an experimental and numerical study to investigate the strengthening effect of GSM on RC beams as well as the time-depended behavior of RC beams with and without strengthening. Reinforced concrete beams without strengthening were used as control beams. For the strengthened beams, both high cord density galvanized steel mesh (HSM) and medium cord density galvanized steel mesh (MSM) were used after which the beams were exposed to Qatar atmospheric environment for different periods of time following 28 days of water curing. Finite element analyses using ABAQUS software were conducted to predict the mechanical behavior of the RC beams with and without strengthening. The results showed an improvement ranging from 46% ~ 57% in the ultimate load of GSM strengthened beams, with a higher initial cracking load ranging from 3% ~ 35% when compared to the unstrengthened beams. On the other hand, the time-dependent effect of the concrete has limited influence on the initial cracking load of both systems (before and after strengthening) while the ultimate load increased gradually with time due to the strength development of concrete. The results obtained from this study are useful in improving the design, construction, and maintenance of RC beams strengthened with GSM laminates.

1. Introduction

Reinforced concrete (RC) structures have been widely used in the construction industry for their relatively low cost and high accessibility [1]. After operating in service for a long durations, structural assets made of concrete deteriorate due to overloading or natural aging under harsh environmental conditions. This may affect the safety and serviceability of these assets, potentially leading to disruption to the society and damage to the economy. Therefore, in order to avoid such scenarios, strengthening of deteriorated RC structures is required with time. In engineering practice, several strengthening methods are available, such as strengthening with metallic plates [2], fiber reinforced polymer (FRP) laminates [1,3], post tensioning [4,5], concrete or steel jacketing [6,7] and injection of epoxy [8,9]. Among these strengthening methods, FRPs has been widely used due to their beneficial properties like corrosion resistance and environmental durability. It is widely acknowledged that FRPs are a good option for enhancing the load-bearing capacity of RC structures and knowledge about FRP mechanical properties has been developing in recent years. Nevertheless, its high cost limits the widespread of its application in engineering practice [1].

A more cost-effective strengthening system, using steel reinforced polymer (SRP) sheets, has been drawing increasing attention in recent years from researchers and engineers around the world. As a type of SRP, embedding galvanized wire steel meshes (GSM) in epoxy was firstly

* Corresponding author at: Department of Civil and Architectural Engineering, College of Engineering, Qatar University, Doha, Qatar (M.Z.E.B. Elshafie); Room 247, Rakentajanaukio 4 A, 02150, Espoo, Finland City, Post code: 02150, Espoo, Finland (W. Lin).
E-mail addresses: weiwei.lin@aalto.fi (W. Lin), melshafie@qu.edu.qa (M.Z.E.B. Elshafie).

https://doi.org/10.1016/j.conbuildmat.2022.127763
Received 29 November 2021; Received in revised form 22 March 2022; Accepted 3 May 2022
Available online 13 May 2022

proposed in the 1990s; in this system the steel wire mesh which has a very high strength is attached with epoxy to concrete surfaces, thus enabling a reliable composite action between the concrete and the strengthening material. Many studies have also been performed in recent years to investigate the real performance of using steel mesh in strengthening RC structures. Xing et al. [10] applied steel wire mesh (SWM) as the strengthening material and embedded the steel mesh in polymer mortar overlay to strengthen T-beams. Five specimens with one-third scale were fabricated and tested under a four-point bending moment. In the study, the strengthening effectiveness of the steel wire mesh system and the negligible effects of loading history on the ultimate load-bearing capacity of strengthened beams were confirmed. Napoli and Realfonzo [11] conducted four-point bending tests on SRP-strengthened slabs using different densities of steel mesh, and the varying parameters were the number of the layers and the density of the steel mesh. The results showed that delamination failure of concrete was found in most of the cases, except for the specimens with one layer of low-density steel mesh in which fracture of sheet was observed. Hawileh et al. [12] studied the effects of medium and high-cord density hardwire steel fibers in strengthening RC beams. The test results showed that the ultimate load-bearing capacity of RC beams has been significantly increased by such light sheets. On the other hand, the ductility of the strengthened beams decreased due to concrete cover delamination. Experimental tests of eighteen small-scale RC beams which were fabricated with self-compacting concrete and strengthened with steel wire mesh system, were conducted by Mohamed et al. [13], and the test results confirmed the increase in the load-bearing capacity due to strengthening. It was also found that reinforcement ratio has a significant effect on the flexural strength. In terms of ductility behavior a different conclusion from Hawileh's [12] study was obtained, which is, SWM strengthened beams normally achieve better performance on ductility compared to control beams. Abdalla et al. [14] proposed a strengthening system with both aluminum alloys (AA) and galvanized steel mesh or CFRP employed where four RC beams were cast and tested under four-point bending. The test results showed that the proposed strengthening system could improve the ultimate load-bearing capacity and ductility effectively. Yuan et al. [15] also proposed a new method for strengthening deteriorated RC beams by employing high-strength steel wire and high ductile engineered cementitious composites (ECC). A total of nine specimens were used to investigate the mechanical performance of this strengthening method, and the effect of the matrix type of the strengthened layer and reinforcement ratio in the strengthened layer were examined. It was found that matrix type of the strengthened layer does not affect the failure mode, and an obvious ductility decrease of strengthened beam was observed. Studies [14] and [15] show the flexibility of the application of SWM in the strengthening of concrete structures.

Based on the existing studies, it is clear that the short-term behavior of this kind of strengthening method was the main focus. Considering the typically long service life of civil engineering infrastructure, durability and time-dependent behavior of RC structures are crucial considerations. Research on the durability or long-term behavior of the RC beams strengthened with steel wire mesh was rarely studied [16]. Al-Khafaji et al. [17] who investigated the durability performance of the bond surface of a steel-reinforced polymer strengthening system, subjected to a harsh environment, falls into this category. In addition, although there are a few numerical simulations that have been conducted to study the durability performance of the FRP-strengthened RC beams (for example the research conducted by Hasani et al. [18]) numerical studies on the durability performance of steel-reinforced polymer strengthened RC beams are still limited. The aim of this paper is to numerically investigate the short-term and long-term behavior of RC beams strengthened using steel mesh laminates; the numerical results are then compared with the experimental results [16] in which testing was conducted to obtain the actual durability performance of the steel mesh-strengthened RC beams. The finite element modelling (FEM) simulations were carried out in this study to characterize the flexural behavior of the strengthened RC beams and to investigate the influence of concrete aging properties and interfacial strength on the behavior of the strengthened beams.

Table 1
List of test specimens.

Exposure time	Exposure condition		
	CB	MSM	HSM
28 days	2	2	2
6 months	2	2	2
12 months	2	2	2
24 months	2	2	2

2. Experimental program

2.1. Description of specimens and loading tests

In order to evaluate the short-term and long-term behavior of the RC beams strengthened with GSM laminates, a total of 24 specimens were designed and manufactured for the loading tests in this study. The details of the test specimens are illustrated in Table 1 and Fig. 1. Eight concrete beams without strengthening were used as control beams (CB). Different cord densities, medium cord density steel mesh (MSM, 4.72 cord/cm) laminates and high cord density steel mesh (HSM, 7.09 cord/cm) laminates were employed in 8 specimens respectively for comparison purposes. The loading tests were performed on two specimens of each category after 28 days, 6 months, 12 months, and 24 months after the concrete casting in order to investigate the short-term and long-term behavior of the specimens.

The dimensions and design details of the beam specimens are shown in Fig. 1. The beams had a section of 140 mm in width and 280 mm in depth. For the HSM specimens, the steel mesh laminate only covered 120 mm of the whole width of 140 mm, which is different from that in MSM specimens, so both groups can have an equivalent reinforcement ratio. The definition of the equivalent reinforcement ratio ρ_{eq} [16] is included here as follows:

$$\rho_{eq} = \rho_s + n\rho_f = \frac{A_s}{bd} + \frac{E_f}{E_s}\frac{A_f}{bd}$$

where:

ρ_s is the reinforcement ratio of main flexural steel,
n is the ratio between elastic modulus of galvanized steel mesh sheet and steel reinforcement,
A_s is the area of main reinforcement,
b and d represent the beam's width and depth,
A_f is the area of steel mesh laminates.

The equivalent reinforcement ratio of 120 mm HSM is 0.0079, which is similar to the reinforcement ratio of 140 mm MSM of 0.0078. Two rebars with a diameter of 12 mm were placed at the beams' tension zone and two rebars with a diameter of 10 mm were employed at the compression zone (Fig. 1). The concrete cover was 25 mm at the top side of the section and 30 mm at the bottom.

The material properties used in this study are shown in Table 2. As for the concrete, the ordinary Portland cement CEM I R42.5, gabbro aggregates of 12.5 ~ 25 mm size and washed sand of 0 ~ 4.75 mm were utilized to cast the concrete.

In this study, the strengthening of concrete beams was performed in three steps: (1) roughening of beam soffits was carried out to enhance the bond between the steel mesh and the concrete beam, (2) mixing the two parts of the epoxy resin and applying it on the roughened concrete surface and (3) placing the steel mesh on the epoxy layer, as shown in Fig. 2.

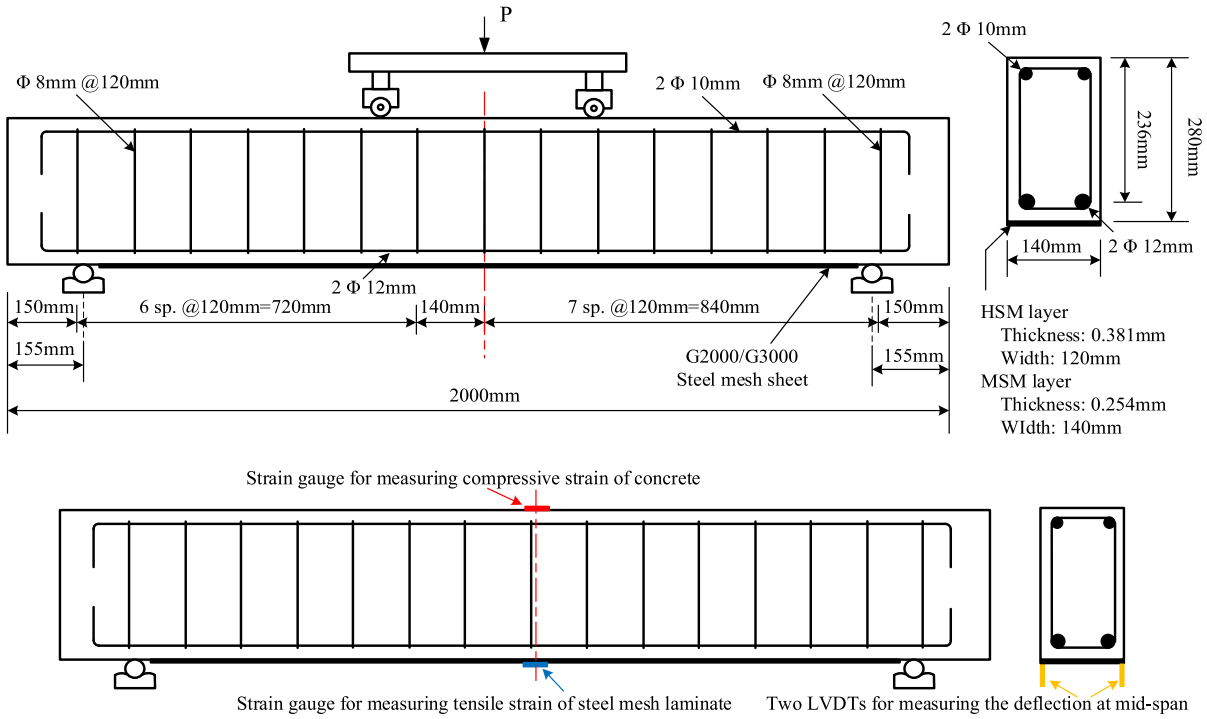

Fig. 1. Size dimensions of the concrete beam and steel mesh laminate.

Table 2
Mechanical properties of materials.

Materials	Compressive strength (MPa)	Tensile strength (MPa)	Elastic modulus (GPa)	Yield strength (MPa)
Concrete	42	4.03	–	–
Steel rebars	–	621	200	536.2
GSM	–	3070	190	–
HSM	–	3070	190	–

2.2. Setup and instrumentation of the loading test

In the loading tests shown in Fig. 3, the RC beams were loaded under four-point bending. The tests were carried using a universal testing machine with a load capacity of 2000kN. The loading was applied using a displacement control method with a rate of 1 mm/min. Two linear variable differential transducers (LVDTs) were placed on both sides of the beam at mid-span to measure the vertical displacement of the beam specimens. In order to investigate the sectional strain distribution and strain development over time, one strain gauge was attached to the top surface of the concrete, two strain gauges were mounted on the surface of the reinforcement, and one strain gauge was attached to the strengthening laminate at mid-span, as shown in Fig. 3.

3. Numerical simulation

3.1. General

The numerical simulation was carried out in three dimensions using the finite element method in the commercial software ABAQUS. Creep and shrinkage were considered in the analysis to take into account the aging effect of the concrete. However, due to the lack of an appropriate built-in creep model in ABAQUS, a user subroutine was developed in this study in Fortran77 to consider the effect of concrete creep and shrinkage based on the model stipulated by CEB fib [29]. Since the creep and shrinkage strains have similar characteristics to thermal strain, the creep and shrinkage strains obtained from the fib model were transferred to thermal strain using the subroutine EXPAN and then submitted to the implicit solver.

3.2. Element types and interactions

The finite element (FE) models developed for the test specimens are shown in Fig. 4. In the developed FE model, the solid element C3D8R, shell element S4R and truss element T3D2 were used to simulate the concrete beam, steel mesh laminate and reinforcing rebars, respectively. The C3D8R element is a frequently used linear solid element with one integration point and eight nodes. To account for the bond relationship between the concrete and steel mesh laminate, cohesive contact was employed to simulate the bonding behavior of the interface.

3.3. Boundary and loading conditions

In this study, the boundary conditions and loading are divided in two stages. The first stage is the period of concrete curing (28 days) followed by the preservation (6 months, 12 months, and 24 months). The second stage is to apply loading till beam failure. To calculate the time-dependent effects in concrete, in the first stage, only gravity of the whole specimen was activated, and the corresponding boundary was set as UY = 0 to simulate the ground support, as shown in Fig. 5 (a). It is noted that the coordinate system X, Y and Z denote the lateral, vertical and beam axis directions, respectively. In the next stage, as shown in Fig. 5 (b), the boundary condition was modified to a simply supported boundary. Degrees of freedom (DOFs) in UX, UY and UZ were restricted in one of the supported lines, while the other support was restricted only in UX and UY. The displacement-controlled loading method was used in the numerical analysis with the load applied at the beam's top surface as shown in Fig. 5 (b).

3.4. Material properties

3.4.1. Concrete

The concrete behavior in compression was assumed to follow the

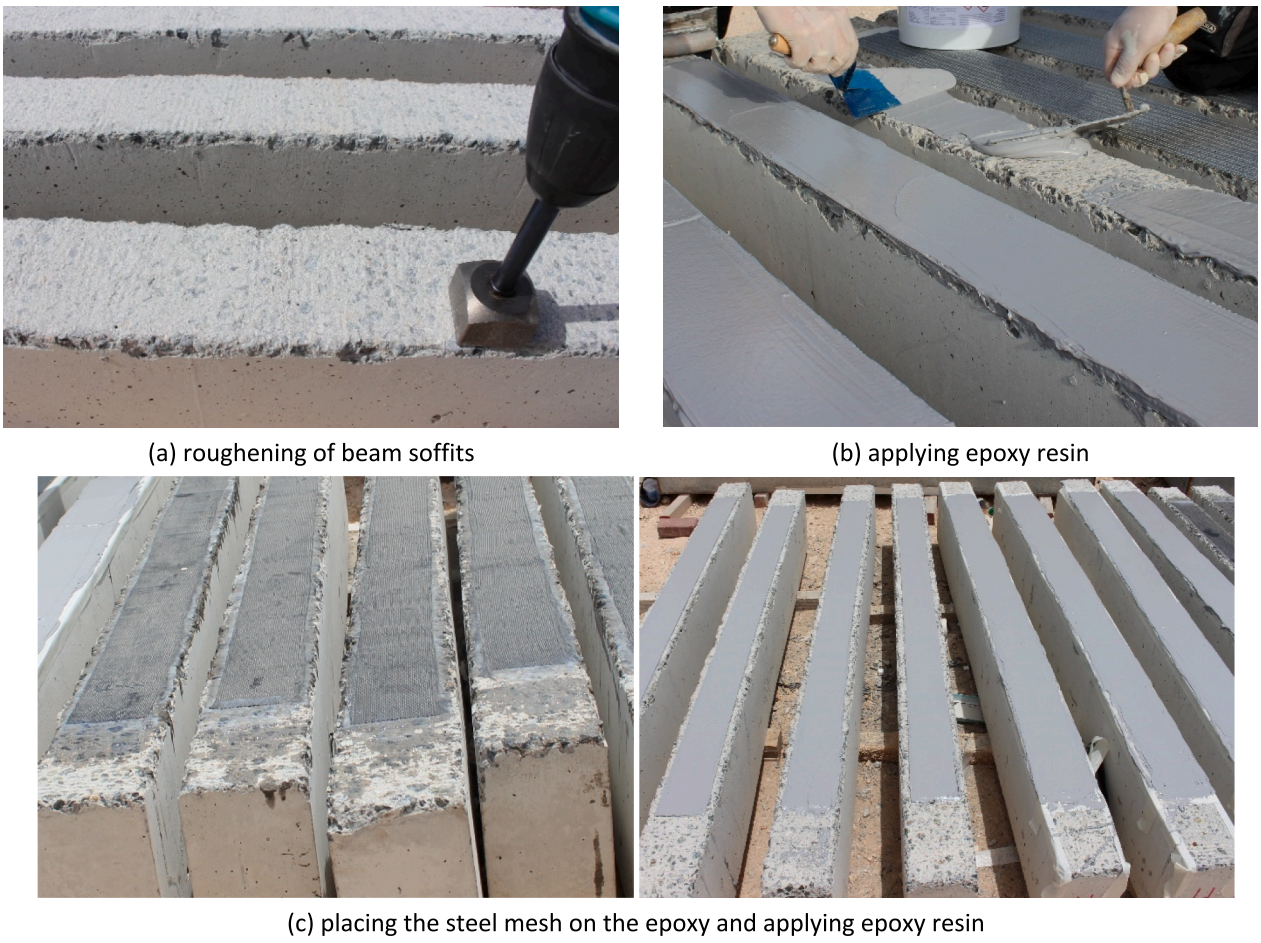

Fig. 2. Strengthening process of the specimens.

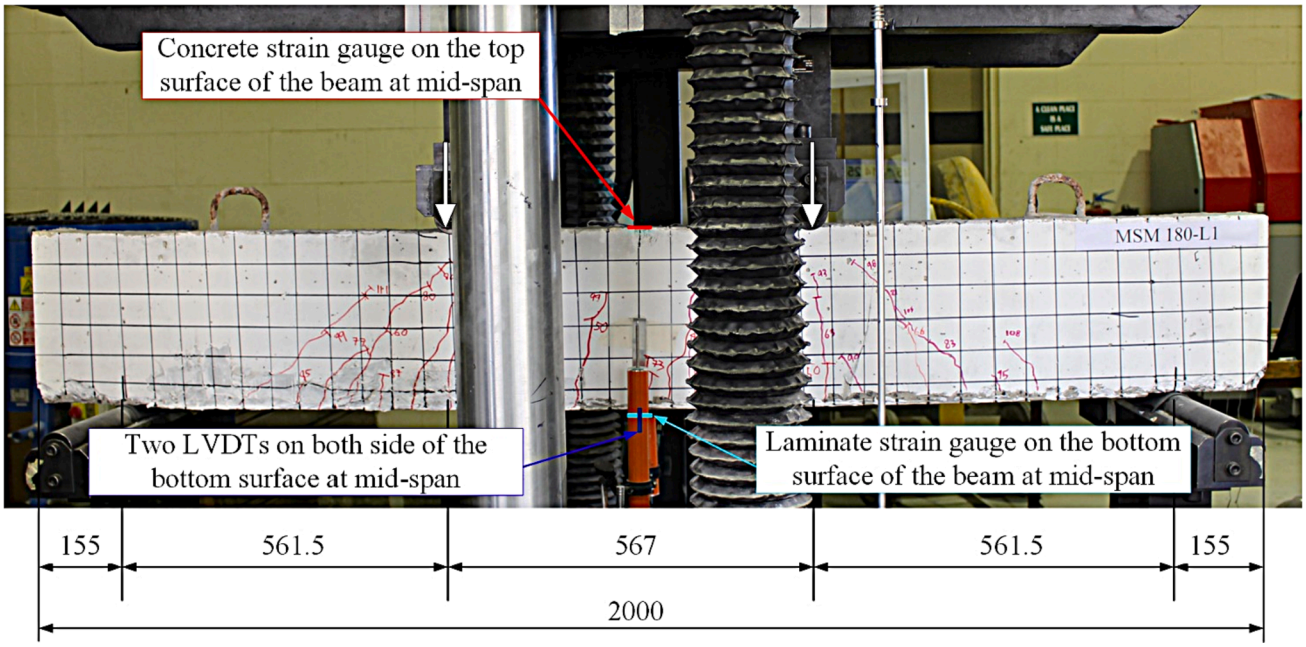

Fig. 3. Test setup.

stress-strain curve, shown in Fig. 6, which is based on the standard specification for concrete structures [28] (JSCE). Based on the material tests, the compressive strength achieved after 28 days was 42 MPa. The elastic modulus of concrete was taken as 29.71 GPa, and the Poisson's ratio was set as 0.17. The curve that describes the compressive behavior of concrete is defined by Eqs. (1)–(3), while the tensile curve is described

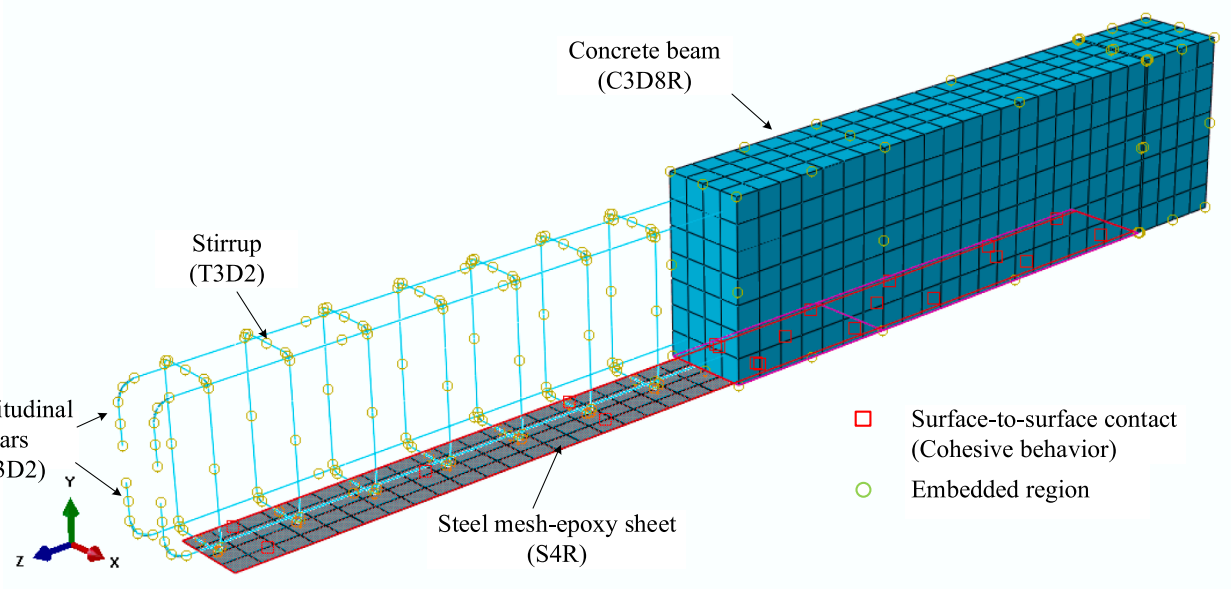

Fig. 4. Finite element model.

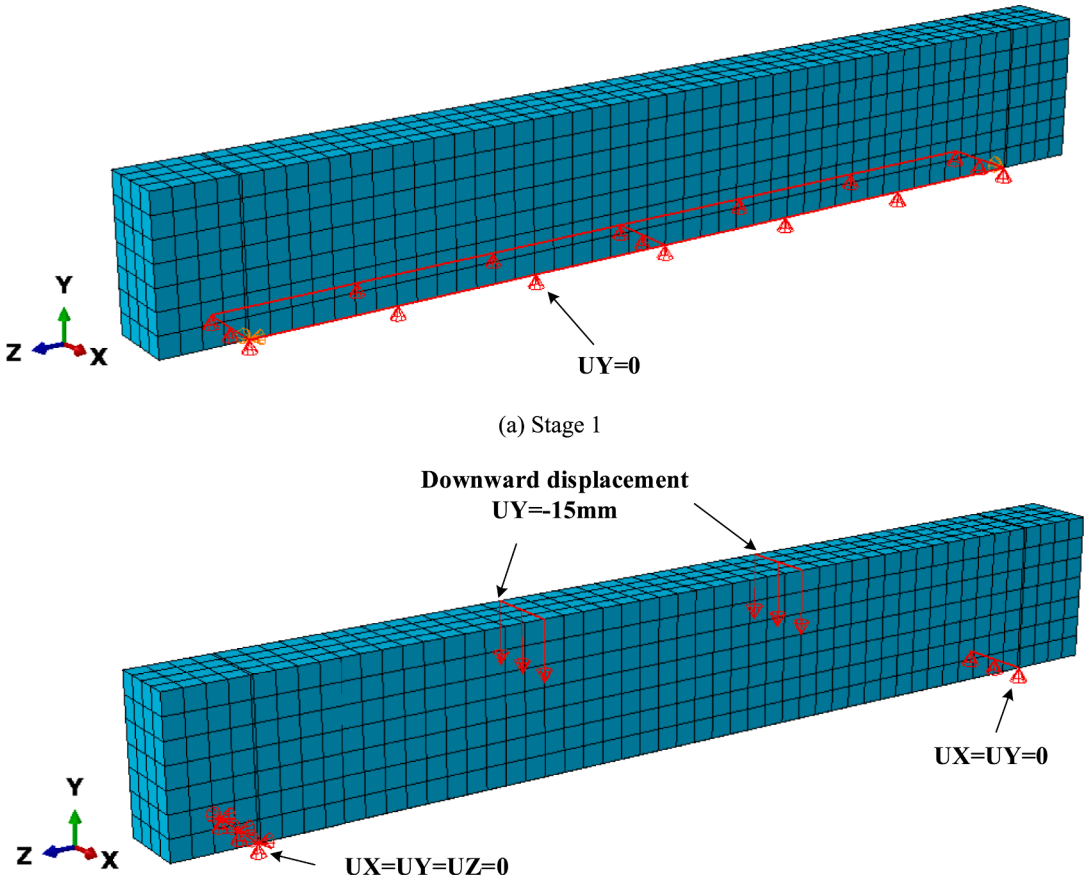

(a) Stage 1

(b) Stage 2

Fig. 5. Boundary conditions of FEA model.

by Eqs. (4) and (5).

$$\sigma_c = k_1 f_{cd} \cdot \frac{\varepsilon_c}{0.002} \cdot \left(2 - \frac{\varepsilon_c}{0.002}\right) \quad (1)$$

$$k_1 = 1 - 0.003 f_{ck} \leqslant 0.85 \quad (2)$$

$$\varepsilon_{cu} = \frac{155 - f_{ck}}{30000}, \ 0.0025 \leqslant \varepsilon_{cu} \leqslant 0.0035 \quad (3)$$

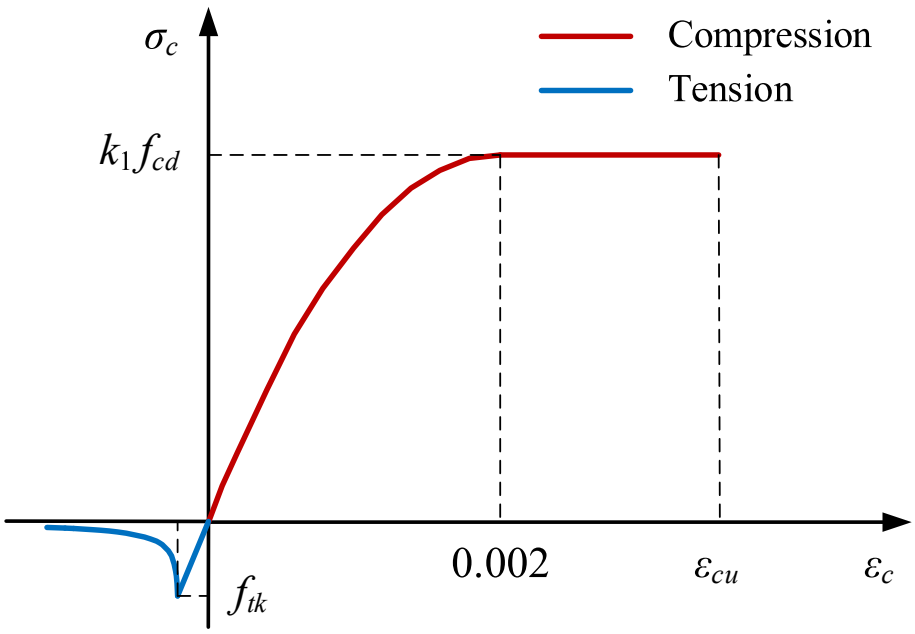

Fig. 6. Material properties of concrete utilized in FEA.

where σ_c, ε_c, f_{cd}, f_{ck}, ε_{cu} denote compressive concrete stress, compressive concrete strain, design compressive strength of concrete, nominal compressive strength of concrete, ultimate compressive strain of concrete, respectively. The item k_1 is a reduction factor.

$$f_{tk} = 0.28 \cdot f_{ck}^{2/3} \tag{4}$$

$$\sigma_t = f_{tk}\left(\frac{\varepsilon_{tk}}{\varepsilon_t}\right)^{0.4} \tag{5}$$

where σ_t, ε_t, f_{tk}, ε_{tk} denote tensile concrete stress, tensile concrete strain, tensile strength of the concrete, tensile concrete strain corresponding to the concrete tensile strength, respectively.

To take account for the time effects (creep) of concrete, Eq. (6) [29] is used to predict the development of concrete strength with time.

$$f_{ck}(t) = \beta_{cc}(t) \cdot f_{ck} \text{with} \beta_{cc}(t) = \exp\left\{ s \cdot \left[1 - \left(\frac{28}{t}\right)^{0.5} \right] \right\} \tag{6}$$

where $f_{ck}(t)$ is the nominal compressive strength at an age t, $\beta_{cc}(t)$ is a coefficient to describe the strength development with time, and s is a coefficient that depends on the strength class of the cement and its value is 0.2 according to the CIB [29].

Since specimens in this research work had different concrete ages and the aging effects could have an influence on the beams' behavior, creep and shrinkage of concrete were considered in the analysis by using the model recommended by the CEB fib model [29]. For the calculation of creep strain, Eq. (7) is employed.

$$\varepsilon_{cc}(t, t_0) = \frac{\sigma_c(t_0)}{E_{ci}} \varphi(t, t_0) \tag{7}$$

where $\varepsilon_{cc}(t, t_0)$ is the creep strain caused by a constant stress $\sigma_c(t_0)$ applied at time t_0, E_{ci} is the modulus of elasticity at the age of 28 days. The creep coefficient $\varphi(t, t_0)$ can be divided into two parts, including the basic creep coefficient $\varphi_{bc}(t, t_0)$ and the drying creep coefficient $\varphi_{dc}(t, t_0)$, as shown in Eq. (8), which is.

$$\varphi(t, t_0) = \varphi_{bc}(t, t_0) + \varphi_{dc}(t, t_0) \tag{8}$$

where the basic creep coefficient $\varphi_{bc}(t, t_0)$ and drying creep coefficient $\varphi_{dc}(t, t_0)$ are defined in Eqs. (9) and (10), respectively. The basic creep coefficient $\varphi_{bc}(t, t_0)$ is expressed as.

$$\varphi_{bc}(t, t_0) = \beta_{bc}(f_{ck}) \cdot \beta_{bc}(t, t_0) \quad \text{with}$$
$$\beta_{bc}(f_{ck}) = \frac{1.8}{(f_{ck})^{0.7}} \quad \text{and} \quad \beta_{bc}(t, t_0) = \ln\left(\left(\frac{30}{t_0} + 0.035 \right)^2 \cdot (t - t_0) + 1 \right) \tag{9}$$

where f_{ck} is the nominal compressive strength at the age of 28 days, t_0 is the age of concrete at loading in days. The drying creep coefficient $\varphi_{dc}(t, t_0)$ is expressed as.

$$\varphi_{dc}(t, t_0) = \beta_{dc}(f_{ck}) \cdot \beta(RH) \cdot \beta_{dc}(t_0) \cdot \beta_{dc}(t, t_0) \quad \text{with}$$
$$\beta_{dc}(f_{ck}) = \frac{412}{(f_{ck})^{1.4}}, \quad \beta(RH) = \frac{1 - \frac{RH}{100}}{\sqrt[3]{0.1 \cdot \frac{h}{100}}}, \quad \beta_{dc}(t_0) = \frac{1}{0.1 + t_0^{0.2}} \tag{10}$$

where RH is the relative humidity of the ambient environment in %. Based on measured data for the average monthly relative humidity at Qatar, a typical maximum value of 70% occurs in January while a typical minimum value of 40% occurs in June. In this study, the higher value of 70% was adopted in the FE analysis. The development of drying creep with time $\beta_{dc}(t, t_0)$ is calculated using Eq. (11), which can be expressed as

$$\beta_{dc}(t, t_0) = \left[\frac{(t - t_0)}{\beta_h + (t - t_0)} \right]^{\gamma(t_0)} \quad \text{with}$$
$$\gamma(t_0) = \frac{1}{2.3 + \frac{3.5}{\sqrt{t_0}}}, \quad \beta_h = 1.5 \cdot h + 250 \cdot \sqrt{\left(\frac{35}{f_{ck}}\right)} \leqslant 1500 \cdot \sqrt{\left(\frac{35}{f_{ck}}\right)} \tag{11}$$

where $h = 2A_c/u$ is the notional size of the member in mm, A_c is the cross-section area and u is the perimeter of the member in contact with the atmosphere.

In order to calculate the shrinkage strain, Eq. (12) is employed and expressed as.

$$\varepsilon_{cs}(t, t_s) = \varepsilon_{cbs}(t) + \varepsilon_{cds}(t, t_s) \tag{12}$$

where the basic shrinkage coefficient $\varepsilon_{cbs}(t)$ and drying shrinkage coefficient $\varepsilon_{cds}(t, t_s)$ were defined in Eqs. (13) and (14), respectively. The

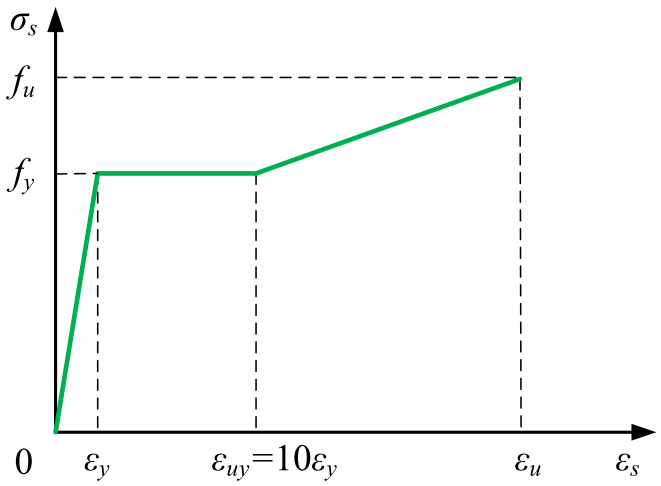

Fig. 7. Material property of steel utilized in FEA.

basic shrinkage coefficient $\varepsilon_{cbs}(t)$ is estimated as.

$$\varepsilon_{cbs}(t) = \varepsilon_{cbs0}(f_{ck})\cdot\beta_{bs}(t) \tag{13}$$

where $\varepsilon_{cbs0}(f_{ck})$ is the basic notional shrinkage coefficient, $\beta_{bs}(t)$ is the time function. The drying shrinkage coefficient $\varepsilon_{cds}(t, t_s)$ is estimated as.

$$\varepsilon_{cds}(t, t_s) = \varepsilon_{cds0}(f_{ck})\cdot\beta_{RH}(RH)\cdot\beta_{ds}(t - t_s) \tag{14}$$

where $\varepsilon_{cds0}(f_{ck})$ the is notional drying shrinkage coefficient, $\beta_{RH}(RH)$ is the coefficient considering the effect of the ambient relative humidity, $\beta_{ds}(t\text{-}t_s)$ is a function describing the time development. The expressions and estimation methods of all these parameters can be found in CEB [29].

3.4.2. Steel reinforcement

In all of the tested specimens, two 12 mm diameter rebars were used as the main flexural reinforcement and two 10 mm diameter rebars were employed at the compression zone. Stirrups with diameter of 8 mm were placed at 120 mm intervals in the shear span as shown in Fig. 1. A trilinear simplified constitutive material model was used for the stress-strain curve of reinforcing rebars and stirrups as shown in Fig. 7.

3.4.3. Steel mesh laminate system

The elastic modulus of steel mesh laminate (steel mesh immersed with epoxy) was taken as 190 GPa, and the ultimate tensile strength was set to 3070 MPa. The Poisson's ratio was taken as 0.3. The thickness of HSM laminate is 0.381 mm and 0.254 mm for MSM laminate. As there was no sign that the steel mesh laminate yielded or failed due to tension in the laboratory tests, the steel mesh laminate was considered as elastomer in this numerical analysis according to the experimental observations.

3.5. Bonding behavior of GSM-concrete interface

In the numerical simulation, the interface between steel mesh laminate and concrete was modelled with surface-based cohesive connection, which simplifies the complicated debonding mechanisms with a macroscopic constitutive law. In this analysis, the bilinear model shown in Fig. 8 was employed to simulate the bonding and debonding behavior on the GSM-concrete interface [19–23].

Few experimental data and models are available to simulate the bonding behavior of the interface between concrete and steel mesh laminate. Based on the tests of Ascione et al. [24,25], shear strength and stiffness were determined. According to Bencardino and Condello [27], it is acceptable that both opening and sliding fracture modes share the same bonding parameters, including initial stiffness, normal or bond strength and fracture energy. In this study, therefore, the normal bonding behavior refers to the parameters obtained by Bencardino and Condello [27] based on the bond-slip model proposed by Lu et. al [26]. The normal bonding strength of the interface is set as the tensile strength of the concrete [21] which is 3.03 MPa, and the corresponding normal deformation is 0.05 mm according to Lu et. al [26], with an initial normal stiffness of 60.6 MPa/mm. The parameters used in FEA are listed

Table 3
Parameters of interface.

Parameters	HSM	MSM
Maximum normal traction component (σ_{max}, MPa)	3.03	3.03
Corresponding separation (s_d, mm)	0.05	0.05
Maximum shear traction component (τ_{max}, MPa)	3.14	3.11
Corresponding separation (s_d, mm)	1.55	1.88
Normal stiffness component (k_0, MPa/mm)	60.60	60.60
Shear stiffness component (k_0, MPa/mm)	2.03	1.65
Maximum separation (s_u, mm)	1.94	2.74

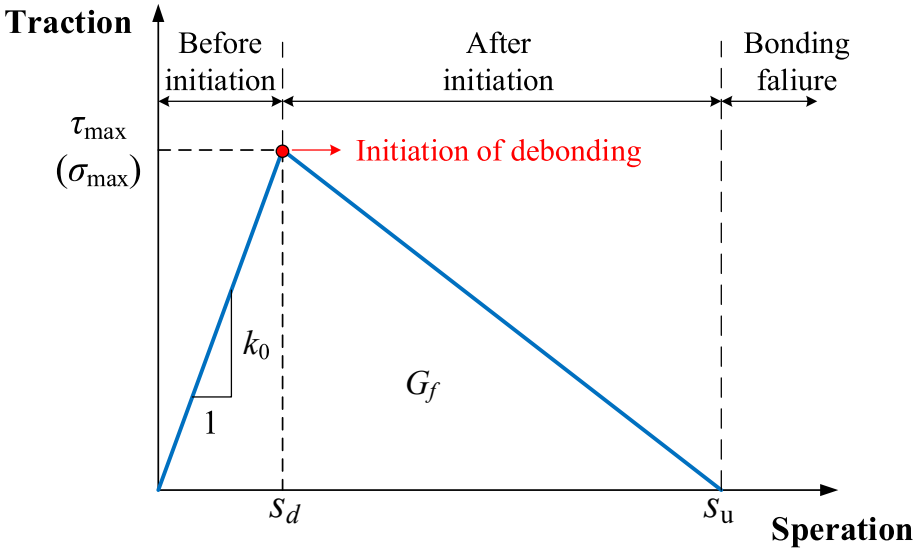

Fig. 8. Bilinear model of constitutive law of laminate-concrete interface.

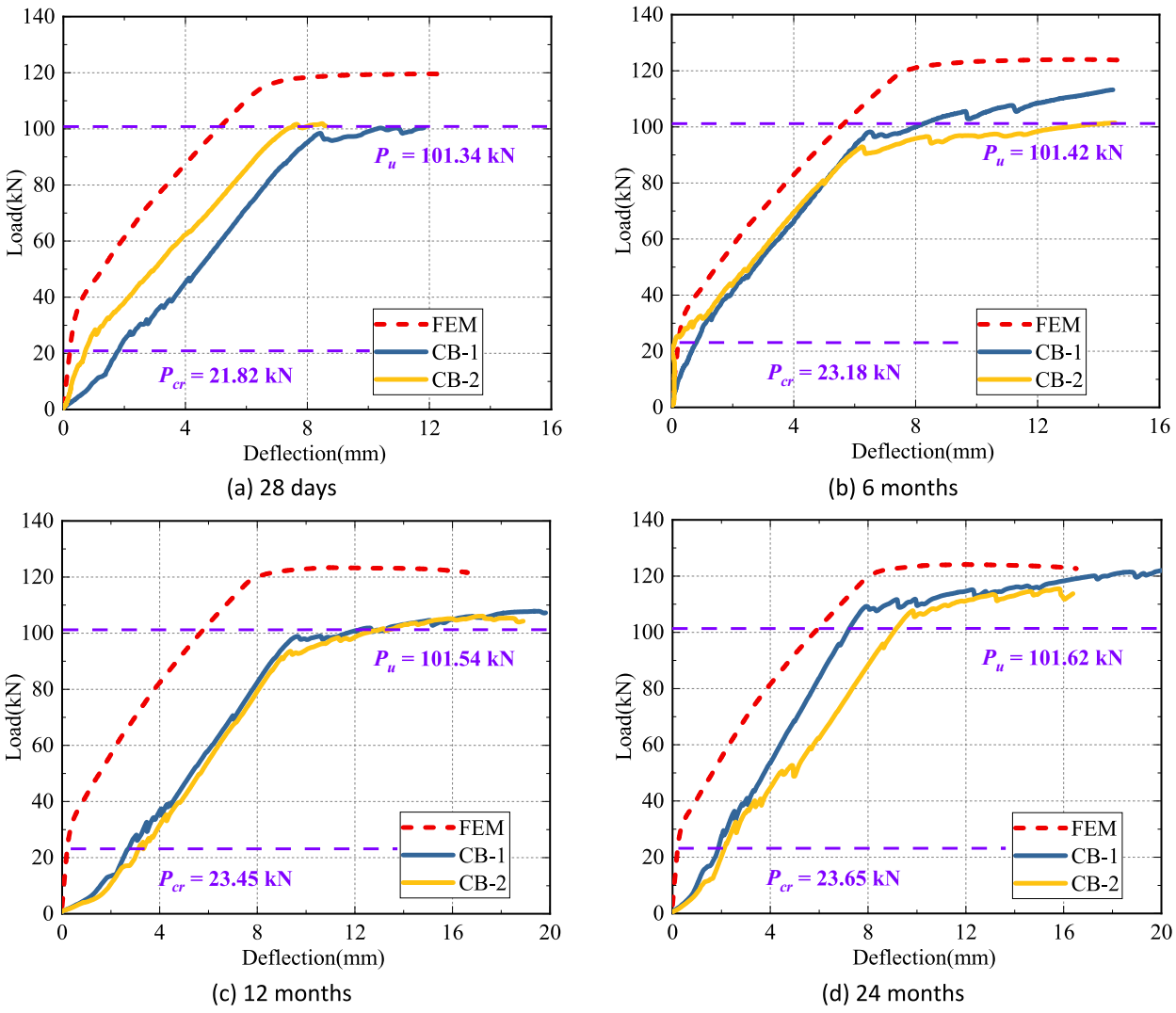

Fig. 9. Load-deflection responses of control beams.

in Table 3.

The adopted damage initiation criterion was defined by Eq. (15).

$$\left\{\frac{\langle\sigma_n\rangle}{\sigma_{\max}}\right\}^2+\left\{\frac{\tau_s}{\tau_{\max}}\right\}^2+\left\{\frac{\tau_t}{\tau_{\max}}\right\}^2=1 \tag{15}$$

where σ_n, τ_s and τ_t denote the normal stress component and two shear stress components, respectively. The Macaulay bracket indicates that the compressive normal stress at the interface does not contribute to the inhiation of debonding. When the Eq. (15) is satisfied, debonding is initiated. The damage evolution was controlled by the fracture energy G_f or the maximum slip displacement.

4. Test and numerical results

In order to assess the effects of the strengthening methods and investigate the time-depended behavior of the tested RC beams before and after strengthening, the loading test results including the applied load versus displacement relationships, applied load versus strain curves on both concrete and steel mesh laminate are reported and discussed.

4.1. Load and deflection responses

The load versus displacement curves of the two control beams (CB-1 and CB-2) are shown in Fig. 9, in which the "Load" is the sum of vertical loads applied on the two loading points, and the displacement is measured from bottom surface of the concrete beam under the loaded section. Taking CB-180 days in Fig. 9 (b) as an example, in the initial loading stage, the applied load increased linearly with the increase of the vertical displacement. A sudden decrease of the beam rigidity was confirmed at CB-2 due to the cracking of the concrete when the applied load was 32.83 kN. Thereafter, the applied load increased gradually as the vertical displacement increased in both CB-1 and CB-2. When the load was around 95 kN, another sudden decrease of the beam rigidity was confirmed, due to the yielding of the reinforcement. After the yield of the main reinforcement, the applied load increased slightly with the vertical displacement, and the loading tests were terminated when the applied load was 113.22 kN in CB-1 and 101.46 kN in CB-2. The predicted numerical results are also provided in Fig. 9. A similar behavior of two typical sudden declines of the rigidity were also confirmed in the numerical analysis at the initial cracking load of 32.02 kN and yield load of 113.38 kN, respectively. For the control beams at an age of 28 days, 12 months and 24 months, obvious difference was observed for the beam rigidity in the initial loading between the test results and numerical results, which could presumably be related to the insufficient preloading prior to testing and possible settlement at the supports. After the initial cracking load, however, relatively good agreement was confirmed for the beam rigidity between the numerical and test results.

The flexural loading performance of all test specimens can be

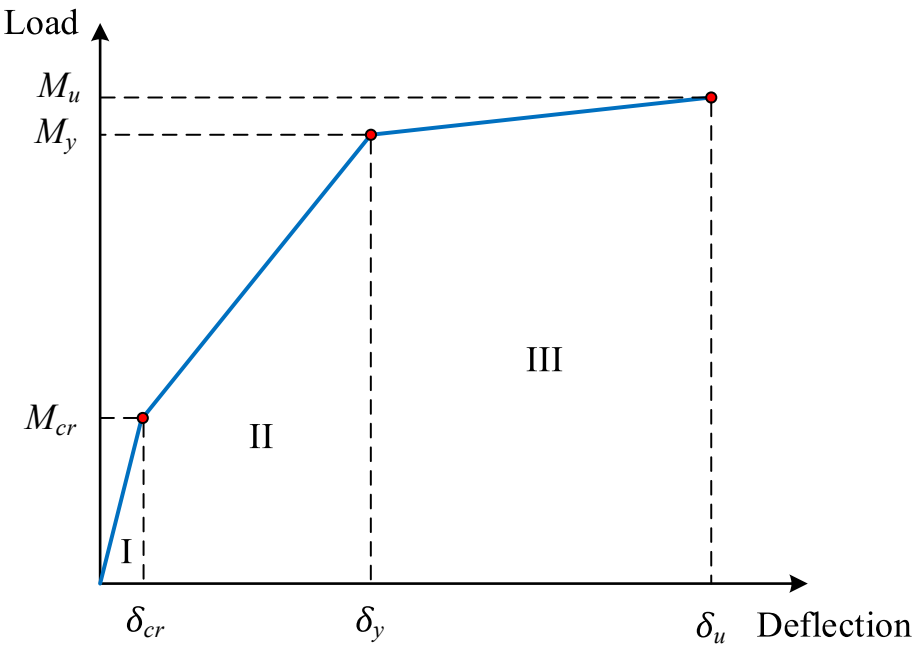

Fig. 10. Typical load-deflection curve of RC beams.

Table 4
Comparison of effective flexural stiffness (kN·mm^{-1}).

Concrete age	Experiment			Theoretical model (error)	Simulation (error)
	CB-1	CB-2	Average		
28 days	5.65	5.55	5.60	7.42 (33%)	6.74 (20.4%)
180 days	6.53	6.06	6.30	7.88 (25%)	6.33 (0.5%)
360 days	6.12	6.28	6.20	7.97 (29%)	6.23 (0.5%)
730 days	7.23	6.29	6.76	8.04 (19%)	6.16 (0.89%)

roughly divided in three stages, similar to conventional RC beams [10]. As shown in Fig. 10, when the loads approach the initial cracking moment M_{cr}, the first stage of loading process is completed. Then with the increase of loading, the flexural reinforcement yields corresponding to the yielding moment M_y. Finally, the load reaches the beam's ultimate moment M_u and then the beam fails.

To validate the developed FE model, the effective flexural stiffness EI_e obtained from experiment, theoretical model and numerical simulation, are compared. In the theoretical model, Eq. (16) was used to calculate the effective moment of inertia I_e.

$$I_e = \left(\frac{M_{cr}}{M}\right)^3 I_g + \left[1 - \left(\frac{M_{cr}}{M}\right)^3\right] I_{cr} \leqslant I_g \quad \text{for} \quad M \geqslant M_{cr} \tag{16}$$

where I_g and I_{cr} denote gross moment of inertia of uncracked section and transformed moment of inertia of cracked reinforced concrete section, respectively. The deflection at mid-span under four-point-bending can be expressed by Eq. (17).

$$\delta = \frac{Pa}{24EI_e}\left(3l^2 - 4a^2\right) \tag{17}$$

where P is the applied load per loading point, l is the span length (1690 mm) and a is the distance of the loading points from the supports (561.5 mm).

For convenience of comparison, slopes of the load-deflection curves in stage II, i.e., P/δ in Eq. (17), are compared and listed in Table 4. It is clear that the effective flexural stiffness obtained from the numerical simulation agree better with the experimental results than that of theoretical model. The errors between simulation and experiment results are mostly below 1%, except for specimens with age of 28 days (20.4%).

The theoretical initial cracking moment M_{cr} and ultimate moment M_u of the control beams were calculated based on Eqs. (18) and (19), respectively, and the corresponding applied load P_{cr} and P_u are also illustrated in Fig. 9.

$$M_{cr} = f_{tk} W_g \tag{18}$$

$$M_u = A_s f_y \left(d - \frac{\beta_1 c}{2}\right) \tag{19}$$

where f_{tk} is the tensile strength of the concrete, W_g is the flexural modulus of an uncracked section, A_s is the total area of the reinforcement, f_y is the yield strength of the reinforcement, d is the effective height of the section, c is the height from the extreme compressive fiber of the concrete to the neutral axis, and β_1 is the ratio of the height of the equivalent rectangular stress block to the height of the neutral axis.

Based on the experimental results, the initial cracking loads were around 28.06 kN for CB-28 days, 32.88 kN for CB-180 days, 26.86 kN for CB-360 days and 31.01 kN for CB-730 days, respectively, while the numerical results showed the average initial cracking load is 29.57 kN which is quite close to the experimental value. With the concrete age increasing, the compressive strength and elastic modulus also increase accordingly, though the enhancing effect is not significant. In addition, the time-dependent effect barely affects the tensile strength of concrete. As shown in Eq. (18), the initial cracking load is influenced by the tensile strength of concrete and flexural modulus of uncracked section. Therefore, on the basis of the aforementioned discussion and experimental results, the time-dependent effects of the concrete have limited influence on the initial cracking loads.

The ultimate loads obtained from experiments were 101.66 kN for CB-28 days, 109.24 kN for CB-180 days, 106.96 kN for CB-360 days and 118.78 kN for CB-730 days, respectively. Basically, the ultimate load gradually increased as the concrete age increases, and this might be mainly due to the development of the compressive strength of concrete with time.

The load versus displacement curves of two HSM strengthened beams (HSM-1 and HSM-2) and two MSM strengthened beams (MSM-1

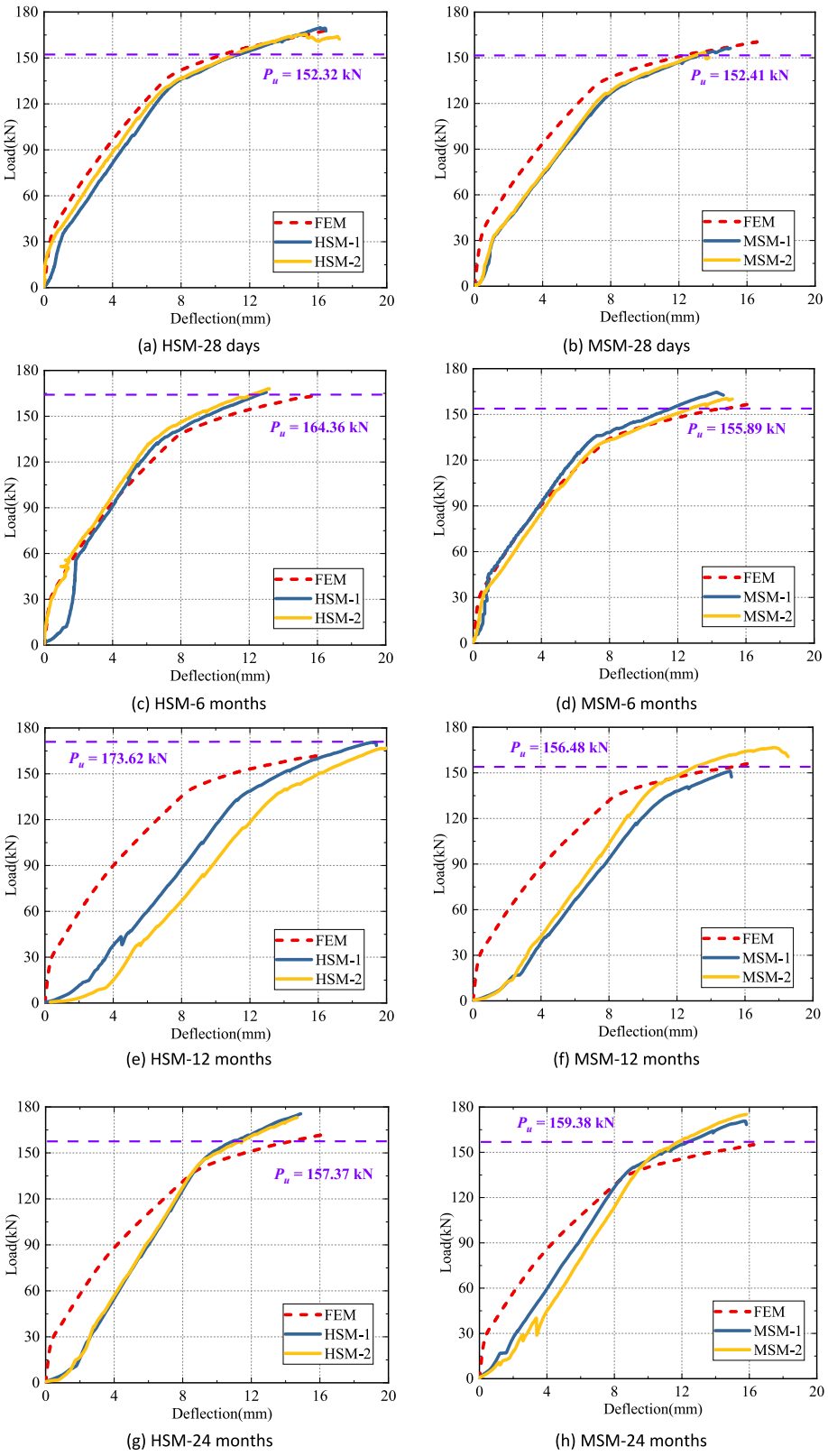

Fig. 11. Load-deflection responses of GSM strengthened beams.

and MSM-2) are shown in Fig. 11, and these curves are trilinear as well. In contrast to the unstrengthened beams, after steel yielding, the applied load increased significantly with the vertical displacement. This is owing to the strengthening effect of the steel mesh laminate. When the main reinforcement yields, the concrete in compression zone could still provide compressive force to resist the external bending moment, as the strain of the extreme compressive fiber of the concrete was around 1000 μ (as shown in Fig. 14) when reinforcement yielded, much smaller than the crushing strain of 3500 μ. Therefore, the application of steel mesh laminate enabled higher utilization rate of the concrete, subsequently

Table 5
Comparison of initial cracking loads (kN).

Concrete age	CB (EXP)	HSM (EXP)	HSM/CB	HSM (FEM)	MSM (EXP)	MSM/CB	MSM (FEM)
28 days	27.44	33.83	1.23	32.15	34.11	1.24	30.57
180 days	29.33	33.84	1.15	28.36	33.61	1.15	28.28
360 days	25.56	36.67	1.43	26.50	32.02	1.25	27.15
730 days	30.27	31.13	1.03	25.31	38.02	1.26	26.28

enhancing the load-bearing capacity of the RC beam specimens.

It is found that for GSM strengthened beams at the age of 28 and 180 days, the FE results of the load-displacement curves are in good agreement with the test results. For the GSM strengthened beams with the age of 12 months and 24 months, obvious differences were observed for the beam rigidity in the initial loading between the test results and numerical results, which could presumably be due to the inaccurate measurement of the vertical displacement in the initial loading stage due to insufficient preloading, similar to those as previously discussed in control beams.

The initial cracking loads obtained from experimental and numerical simulation have been summarized in Table 5. It can be observed that the initial cracking load of the RC beam after strengthening increased about 3% to 35% compared to that of before strengthening, which confirm the strengthening effect of the steel mesh laminate on postponing the occurrence of concrete cracking. Similar to the control beams, the time-dependent effect of the concrete barely affects the initial cracking loads of the GSM strengthened RC beams.

To calculate the ultimate load capacity of the GSM strengthened beam, the ACI 440. 2R-17 [30] was used. The predicted bending moment capacity can be expressed as Eq. (20).

$$M_u = A_s f_y \left(d - \frac{\beta_1 c}{2}\right) + \psi A_{gsm} f_{gsm,e} \left(h - \frac{\beta_1 c}{2}\right) \tag{20}$$

where ψ is the strength reduction factor of 0.85, A_{gsm} is the sectional area of the galvanized steel mesh laminate, $f_{gsm,e}$ is the effective stress in steel mesh laminate and h is the height of the section. The calculation of $f_{gsm,e}$ is illustrated in Section 4.3. The predicted ultimate loads and experimental results are listed in Table 6. It is obvious that the predicted ultimate loads are in good agreement with the experimental results. The errors between the predicted and experimental values vary from 1% to 9%. Therefore, it is accurate enough to use the prediction model of ACI 440. 2R-17 to calculate the ultimate load-carrying capacity of the GSM strengthened RC beam. By comparing the ultimate loads of GSM strengthened and unstrengthened beams, it can be found that the ultimate loads were around 46% ~ 57% larger after strengthening, which significantly confirm the strengthening effect of steel mesh laminate on enhancing the load-bearing capacity of RC beams. Moreover, it can be observed that the ultimate load of the GSM strengthened beams gradually increased with the concrete age as well, similar to that of the control beams.

4.2. Concrete strain development

Fig. 12 shows the results of concrete strain development of CB

Table 6
Comparison of predicted ultimate loads and experimental results (kN).

Concrete age	HSM (EXP)	HSM (PRED)	Error	MSM (EXP)	MSM (PRED)	Error	CB (EXP)
28 days	165.09	152.32	−7.7%	154.49	152.41	−1.3%	101.66
180 days	166.98	164.36	−1.6%	162.60	155.89	−4.1%	109.24
360 days	170.45	173.62	1.8%	159.00	156.48	−1.6%	106.96
730 days	172.95	157.37	−9.0%	174.29	159.38	−8.6%	118.78

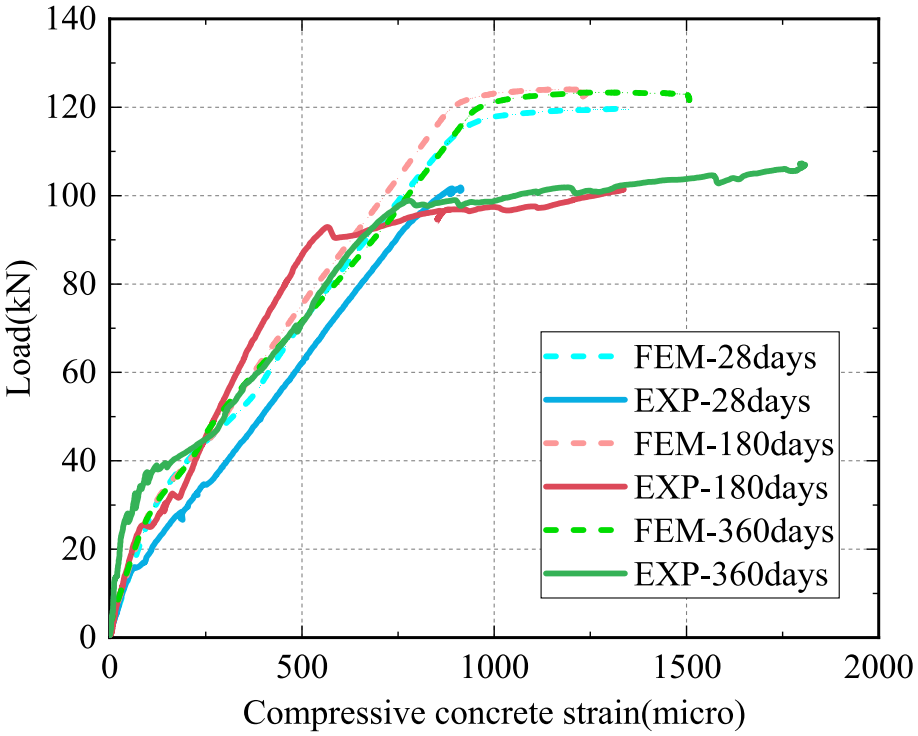

Fig. 12. Load-concrete strain responses of unstrengthened specimens.

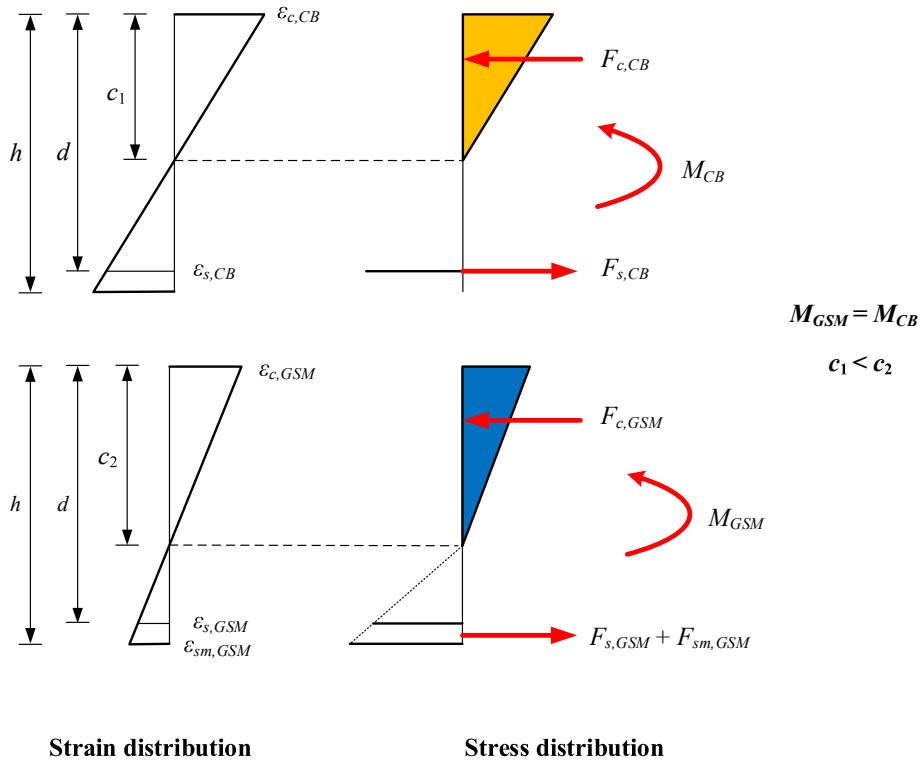

Fig. 13. Section analysis before and after strengthening.

specimens at different loading. The measured section was located at the beam's mid-span and the compressive strain of the concrete at the beam's top surface is the main focus in this section. Comparing the concrete strain development before cracking and taking the applied load of 20 kN as an example, it can be found that compressive strain of concrete reduced from 108.9 μ in CB-28 days to 57.27 μ in CB-180 days, then reduced to 26.29 μ in CB-360 days. The ultimate compressive strains of concrete were below 2000 μ, and this indicates the failure of the unstrengthened beams was due to the crushing of concrete near the loading position, which can be confirmed from the failure mode (Section 4.4).

Comparing the concrete strain development between the GSM strengthened and unstrengthened beams, it could be observed that at the same loading level, the strain of the extreme compressive fiber of concrete in the GSM strengthened beams was slightly lower than of the strengthened beam. Assuming the same external bending moment was applied on a GSM strengthened beam and an unstrengthened beam respectively, the strain distributions of these two cases are shown in Fig. 13. In order to obtain the same resultant bending moment, $\varepsilon_{c,CB}$ should be lower than that of $\varepsilon_{c,GSM}$.

Comparing the concrete strain development between HSM strengthened and MSM strengthened beams, there is no obvious difference that could be observed. This is presumably because of the similar equivalent reinforcement ratio (0.0079 for HSM laminates and 0.0078 for MSM laminates). The maximum compressive strain of concrete at failure in all specimens was lower than 2500 μ, which indicates the concrete crushing at the compression zone was not the leading factor that controls the failure of the strengthened beam.

Fig. 14 shows the experimental and predicted FE results of the concrete strain development of the GSM strengthened specimens at different concrete ages. In general, the simulation results agreed well with the experiment results, though the rigidities of the numerical models were slightly higher than the measured results in specimens with the age of 6 months and 12 months.

4.3. Steel mesh laminate strain development

The comparison of numerical and experimental results of the load versus steel mesh laminate strain curves for the GSM strengthened beams are shown in Fig. 15. In the initial loading stage, the strain of steel mesh laminate increased linearly with the increase of the applied load. The increasing of the strain was accelerated after the occurrence of concrete cracking and the decrease of the beam's rigidity. When the applied load reached the yielding load which was around 130 kN for both HSM and MSM specimens, the increasing rate of the strain in the steel mesh laminate increased further. Thereafter, the strain of steel mesh laminate increased gradually as the applied load increases in all GSM strengthened beams until the ultimate load was reached. Most of the comparisons showed good agreement between the simulation and experimental results, which provides good confidence in the accuracy of the simulation results of the steel mesh laminate's strain development.

It can be observed that the maximum strains of steel mesh laminate in all the specimens do not exceed 10,000 μ, around 36% less than its ultimate tensile strain of 13,950 μ. Therefore, it is appropriate and accurate enough to treat the steel mesh laminate as elastomer in the FE analysis. The average ultimate tensile strain of the steel mesh laminate was 8326 μ for HSM-28 days, 8904 μ for HSM-180 days, 5971 μ for HSM-360 days, 9484 μ for HSM-730 days, 6464 μ for MSM-28 days, 8023 μ for MSM-180 days, 9232 μ for MSM-360 days and 7116 μ for MSM-730 days. Therefore, the effective stress $f_{gsm,e}$ in the steel mesh laminate is the ultimate strain times the elastic modulus of steel mesh laminate (190 GP), resulting in an average effective stress of 1464.6 MPa for the HSM strengthened beams and 1552.5 MPa for the MSM strengthened beams respectively. The value of effective stress in the steel mesh laminate can be used to compute and evaluate the attained ultimate load of the GSM strengthened beam specimens.

4.4. Failure modes

In this experimental program, all specimens failed in flexure, but two different failure modes were observed between specimens before

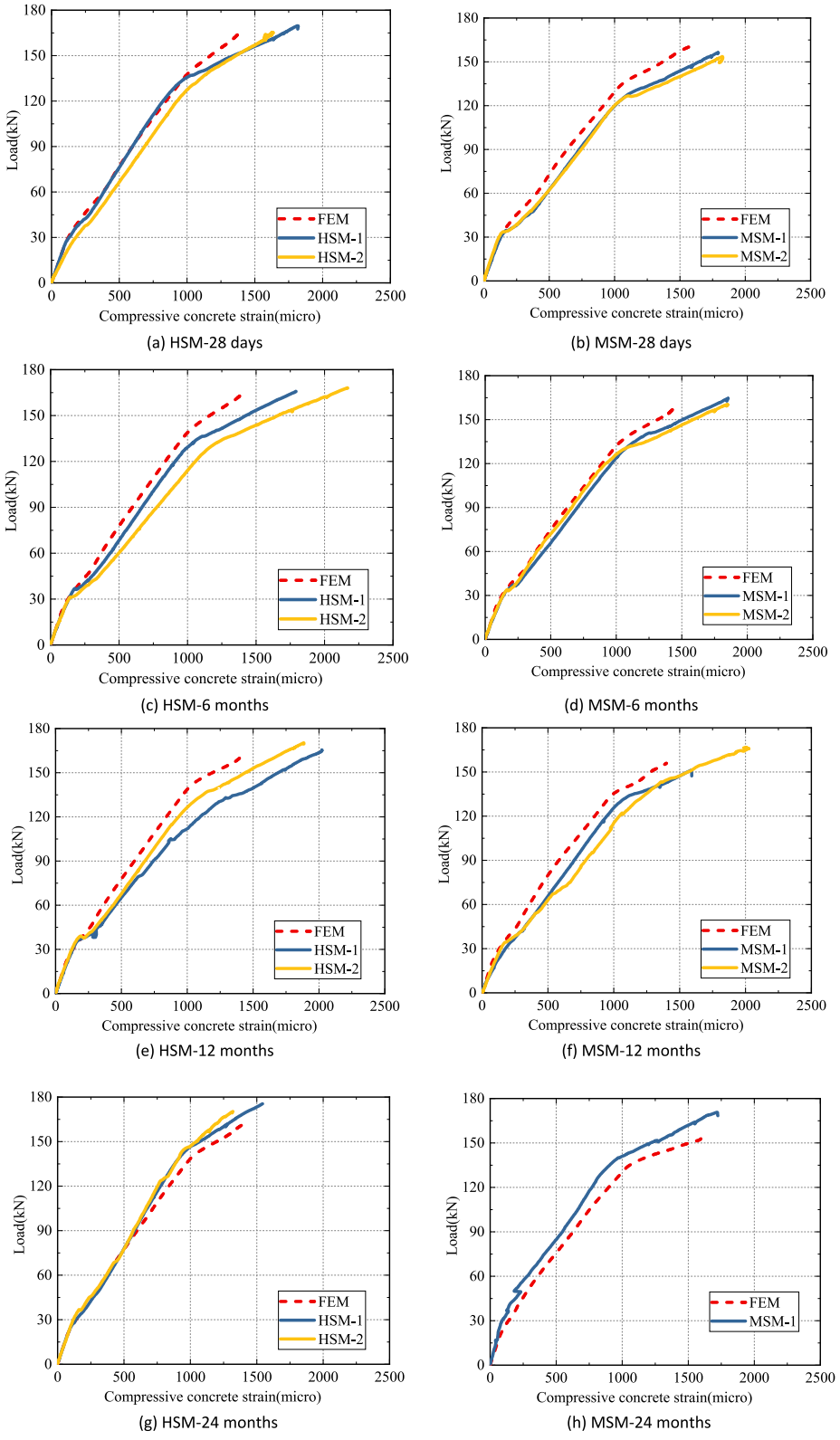

Fig. 14. Load-concrete strain responses of GSM strengthened beams.

(control beams) and after strengthening. The control beams were typically failed with yielding of main reinforcement followed by concrete crushing in compression, while the strengthened beams were mainly failed by concrete delamination (concrete cover separation) that mostly occurred near the steel mesh laminate-concrete interface. The test specimens CB-28 days and CB-180 days after the loading test are shown in Fig. 16.

Fig. 17 (a) and (b) shows the failure modes of the HSM strengthened specimens. For the specimen with a concrete age of 28 days and 180 days, it failed due to the delamination of concrete cover at the end of the steel mesh laminate, rather than excessive slip between HSM laminate and concrete interface, which proves the high bond performance of this

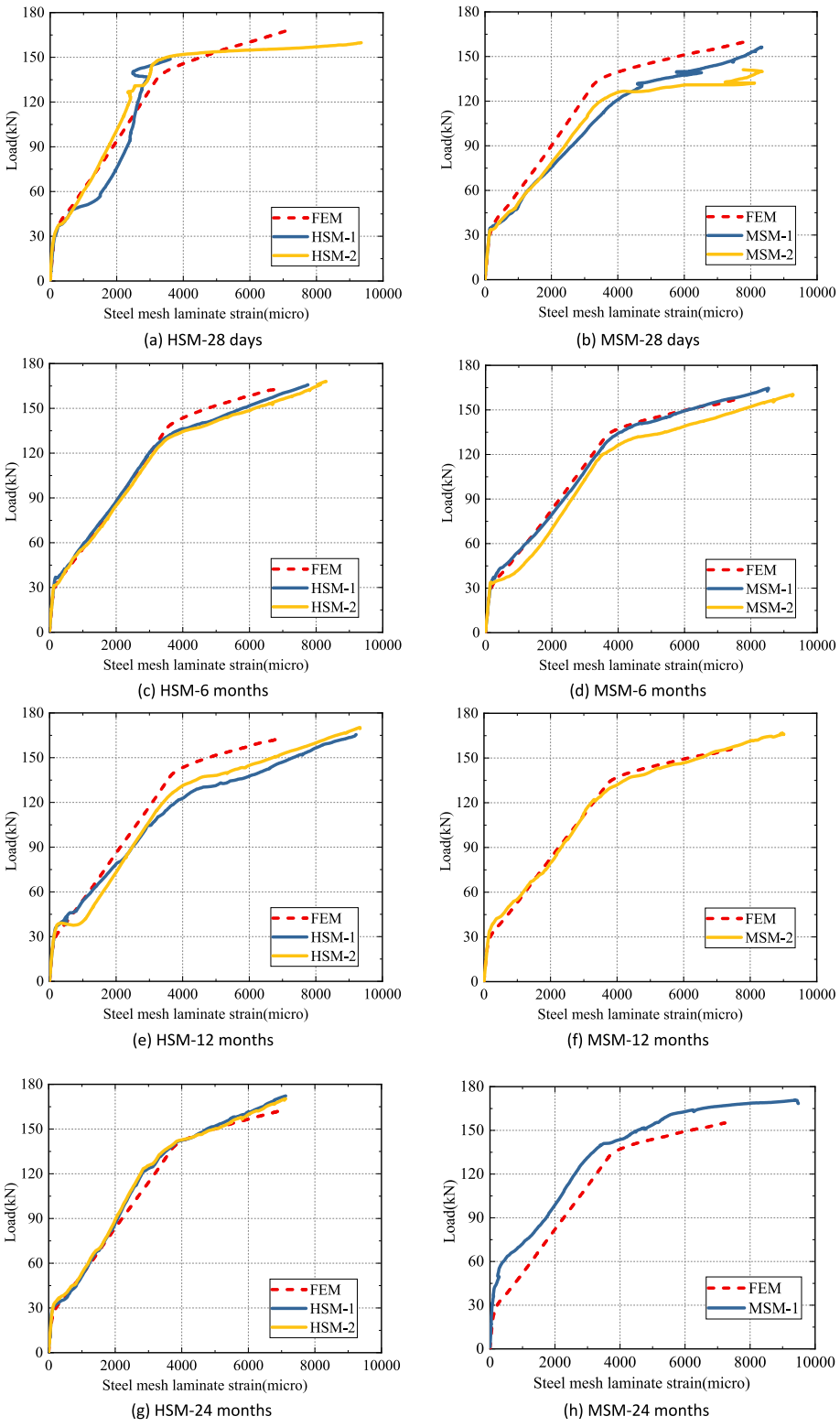

Fig. 15. Load-steel mesh laminate strain responses of GSM strengthened beams.

strengthening method. After being strengthened, cracks near the support were mainly caused by the huge shear force along the interface between the concrete and steel mesh laminate, as can be seen from Fig. 17 (a) and (b). Fig. 17 (c) also shows that the damage initiation does not occur until the beam failure (damage index CSQUADSCRT was lower than 1 over the interface). Regarding the crack pattern Fig. 17 (d) gives the distribution of principal strain of the concrete under different applied loading stages. As commonly known, concrete cracks initiate due to excessive maximum principal strain and propagates along the direction of the minimum principal strain. So, the distribution of principal strain is used instead to illustrate the crack pattern. The cracks can be classified into two categories: bending cracks and shearing cracks. In the pure bending zone, the direction of maximum principal strain is parallel to the beam axis, so the bending cracks propagate along the vertical direction

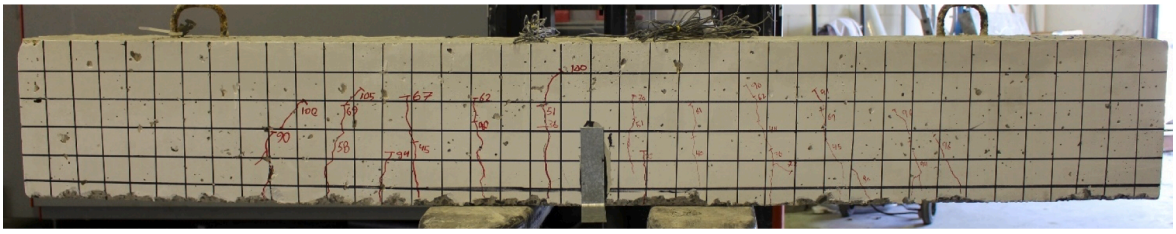

(a) CB-28 days

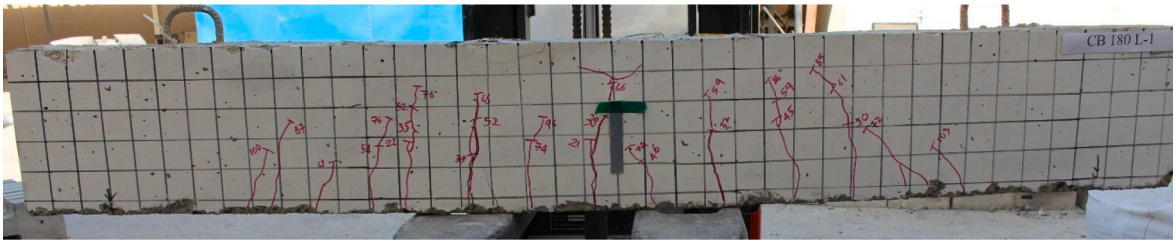

(b) CB-180 days

Fig. 16. Failure mode of control beams.

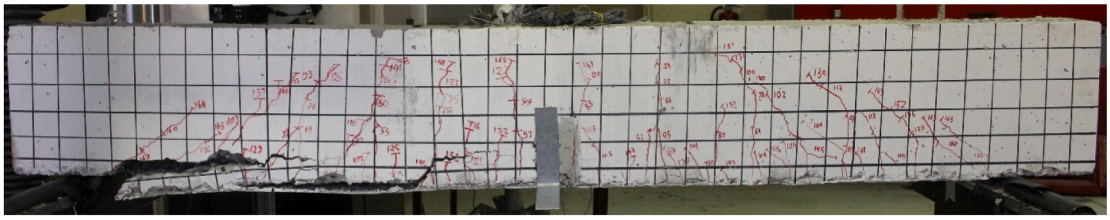

(a) HSM-28 days

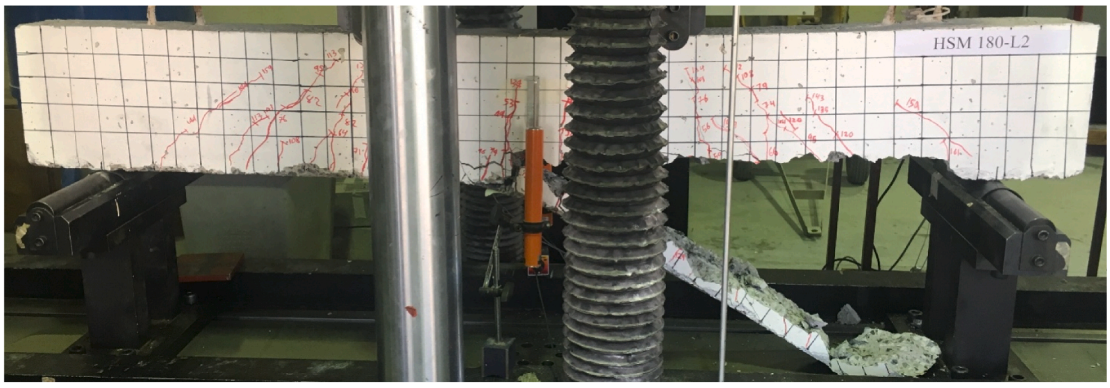

(b) HSM-180 days

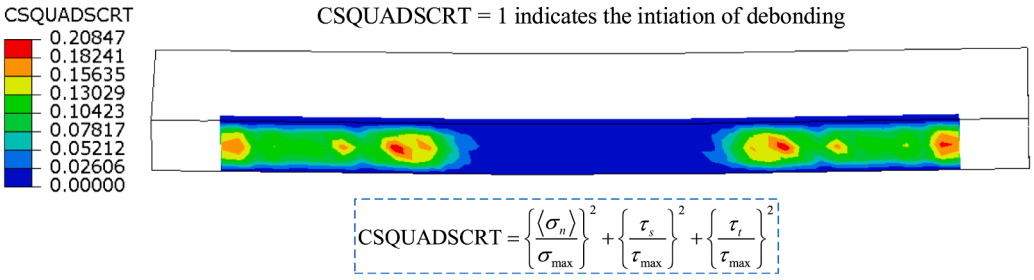

(c) damage index on the interface at failure (HSM-28 days)

Fig. 17. Failure mode of HSM strengthened beams.

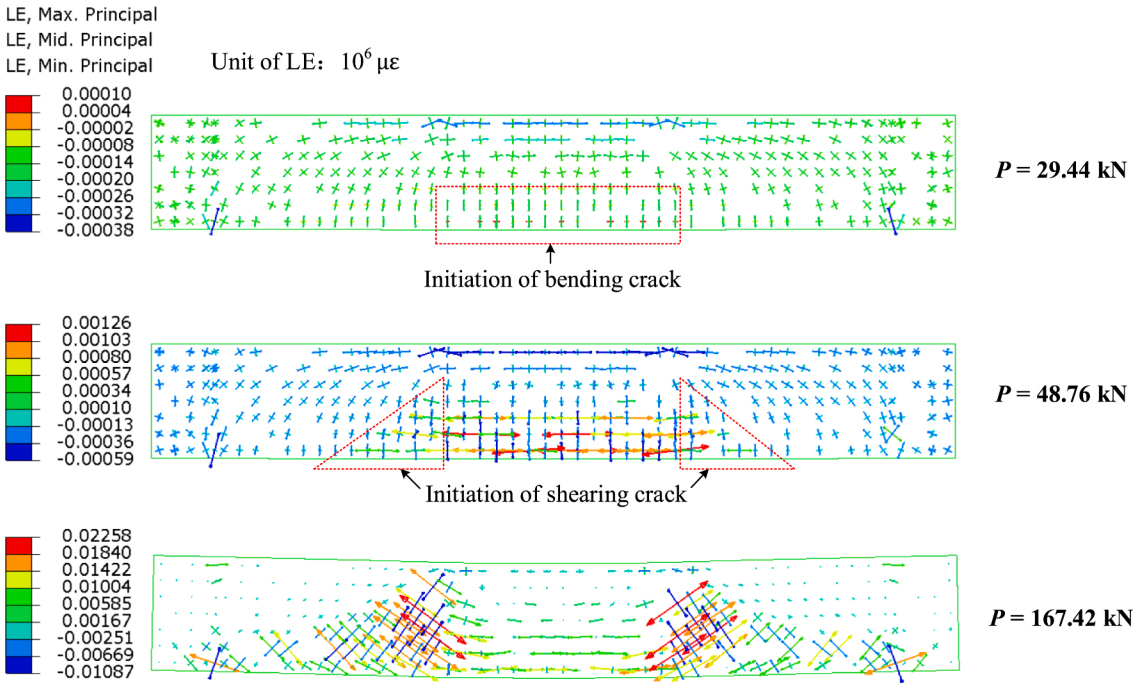

(d) distribution of principal strain (HSM-28 days)

Fig. 17. (*continued*).

(a) MSM-28 days

(d) MSM-180 days

Fig. 18. Failure mode of MSM strengthened beams.

(perpendicular to the beam axis). In the shear span, combined action of shear force and bending moment was applied, and the direction of maximum principal strain is inclined, resulting in shearing cracks propagating, approximately, towards the loading points.

Fig. 18 shows the MSM strengthened specimens after failure. For MSM-180 days, it can be observed that the concrete near the edge of the steel mesh laminate delaminated due to excessive stress concentrations. In contrast with the MSM-180 days, extensive bonding failure of steel mesh laminate occurred in MSM-28 days, which was rarely observed in other GSM strengthened RC beams. As shown in Fig. 15 (b), when the applied load was 132.14 kN, the tensile strain of steel mesh laminate suddenly dropped from 8112 μ to 7271 μ, indicating the occurrence of bonding failure. Then, the strain gradually increased again with the increase in applied loading. When the applied load reached 139.89 kN,

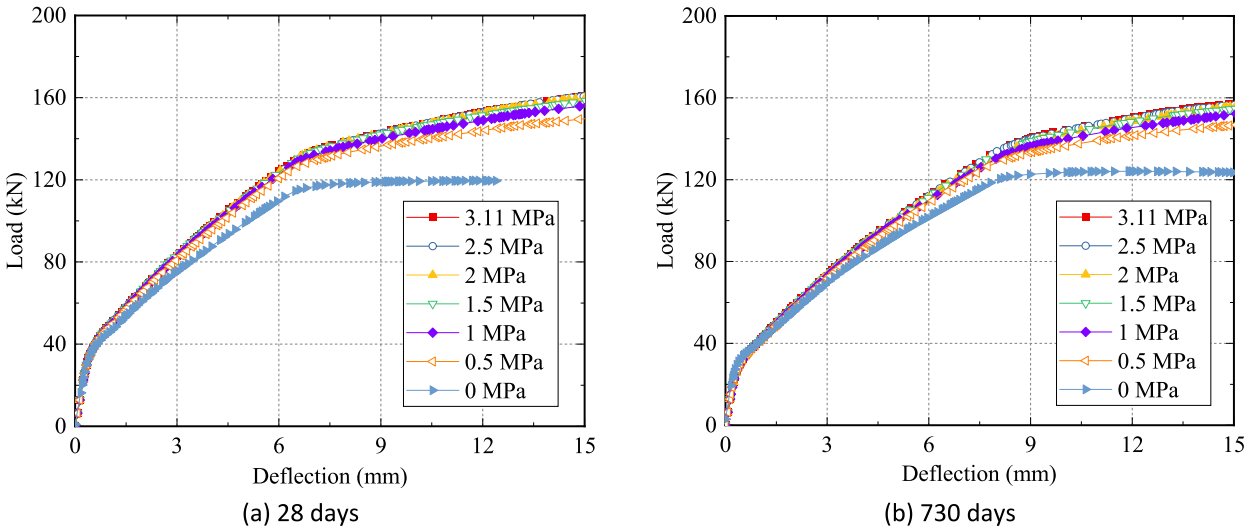

Fig. 19. Load-deflection responses of MSM strengthened beam with different bond strengths.

the strain of steel mesh laminate decreased again from 8346 μ to 7808 μ, which shows the progressive bonding failure of the steel mesh laminate. This is presumably the reason why the ultimate load of MSM-28 days was just 5% lower than that of MSM-180.

5. Parametric study

In this section, effects of interfacial bond strength, dimensions of the steel mesh laminate, concrete creep and shrinkage are discussed. In subsections 5.1 and 5.2, the MSM-strengthened beam was set as the base model, using the interfacial parameters presented in Table 3.

5.1. Effect of the interfacial bond strength

For GSM strengthening method, load transmission from the concrete to the steel mesh laminate is the fundamental aspect in ensuring the strengthening effect. However, the effect of the bond strength on the strengthening performance is still unclear and needed more investigation. In order to figure out the effect of bond strength, a sensitivity analysis was conducted where typical interfacial bond strength values of 0.5 MPa, 1.0 MPa, 1.5 MPa, 2.0 MPa, 2.5 MPa were assumed on the steel mesh laminate-concrete interface.

The simulation results are shown in Fig. 19. It can be observed that, interfacial bond strength had little effect on the rigidity of the beam; this was presumably because the strength contribution of the steel mesh laminate is not significant compared to the uncracked beam section as the whole concrete section remains effective before concrete cracking. With the decrease of interfacial bond strength, the yield load and the corresponding deflection decreased gradually. This was the result of the weakened composite action between the concrete and the strengthening material (given the shear capacity of the interface has been decreased). At an interfacial bond strength decreased to 0.5 MPa, the deflection of MSM strengthened beam at yield was approximately equal to that of the unstrengthened beam, although the yield load was still around 10% larger than that of unstrengthened beam.

In engineering practice, the interface bond between the

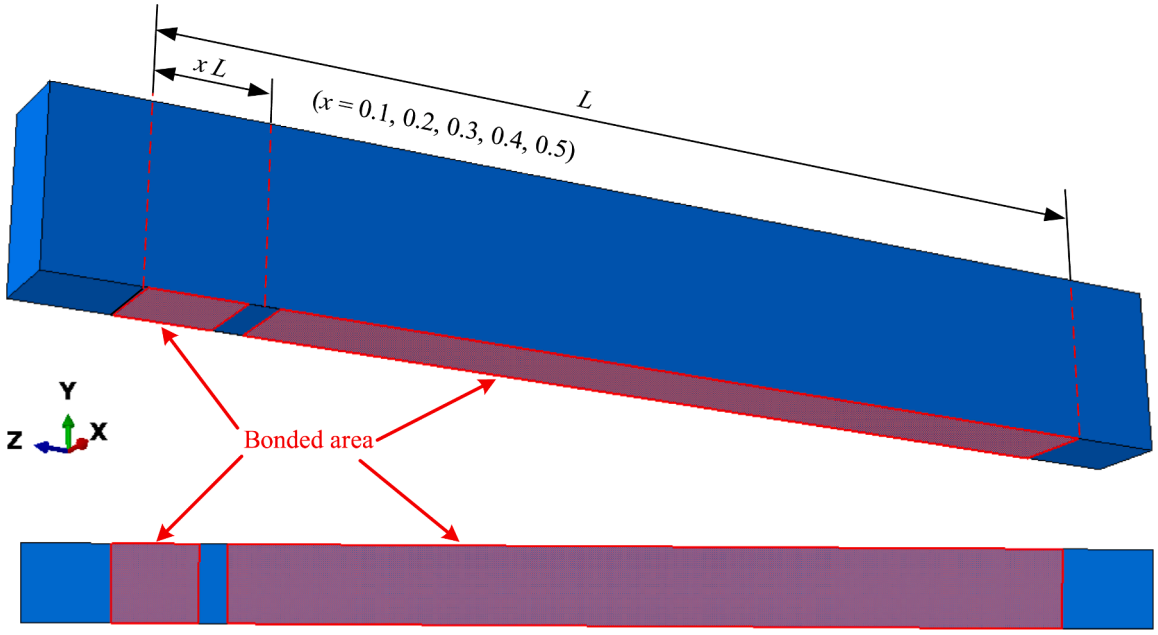

Fig. 20. Illustration of locations of debonded area.

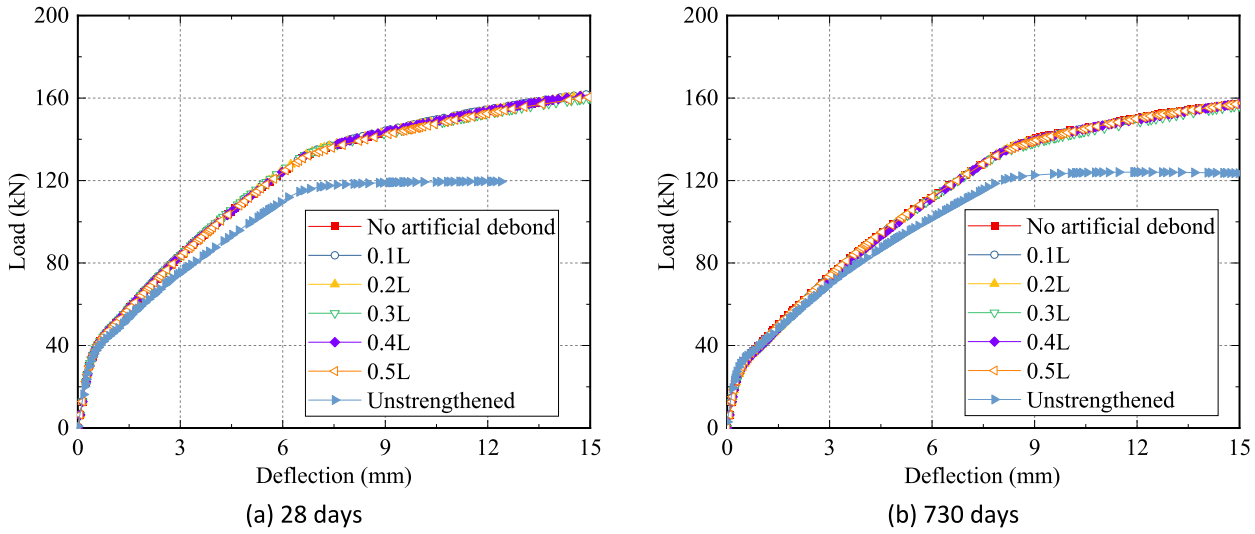

Fig. 21. Load-deflection responses of MSM strengthened beam with different artificial debond locations.

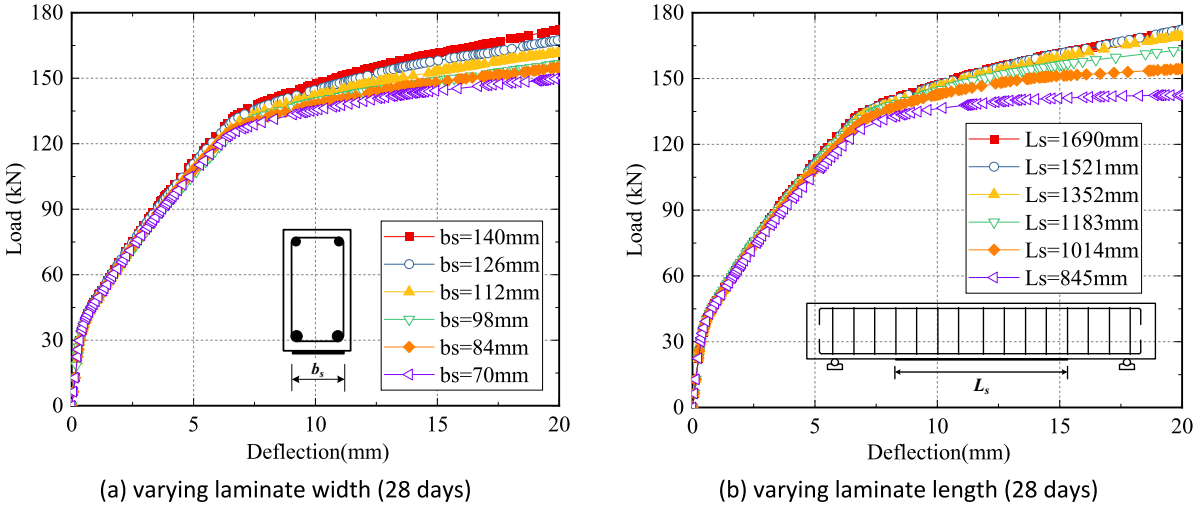

Fig. 22. Load-deflection responses of strengthened beam with different steel mesh laminate dimensions.

strengthening material and the concrete beam will not be perfect (as assumed above) - localized regions with little or no bonding could occur during the strengthening process of the beam. In order to investigate this effect, debonded strips (50 mm in the longitudinal direction running across the width of the beam) were set at different locations (0.1 *l*, 0.2 *l*, 0.3 *l*, 0.4 *l*, 0.5 *l*) as shown in Fig. 20 with a separate FE simulation run for each of the locations shown. The reason why set 50 mm as the length of debonded strips in the longitudinal directions was that, the gabbro aggregates of the concrete in this test was maximum 25 mm and to amplify the effect of localized debond, twice the maximum dimension of gabbro aggregates was used.

The simulation results are shown in Fig. 21. It can be observed that the location of the local artificial debonded strips had little effect on the load bearing capacity of the GSM strengthened beam. Since the debond areas were relatively small, the interfacial stresses in the bonded regions would not increase significantly enough, following stress redistribution, to trigger further debonding; hence, the influence is limited.

5.2. Effect of dimensions of steel mesh laminate

When using the strengthening material in practice, the detailed dimensions of the steel mesh laminate may vary within a given range. The effect of the dimensions of the steel mesh laminate on the performance of a strengthened beam is worth further investigation. In this study, different width and length of the steel mesh laminates were set in the numerical simulation to evaluate the dimension effect of the strengthening material.

First, different widths of steel mesh laminates b_s (70 mm, 84 mm, 98 mm, 112 mm and 126 mm) were investigated and the simulation results are presented in Fig. 22 (a). The comparisons show that decreasing the width of the steel mesh laminate reduced the yield and ultimate loads of the beam. Varying the width of the steel mesh laminate from 0.5*b* to 1*b* decreases the yield and ultimate loads by 5.5% and 13.1%, respectively.

In addition, different lengths of steel mesh laminates L_s (840 mm, 1008 mm, 1176 mm, 1344 mm and 1512 mm) were investigated and the results are presented in Fig. 22 (b). It can be observed that when the length reached around 1352 mm (0.8*l*), any further increase did not have a significant effect. This might be due to different 'effective areas' in the shear spans. In four-point loading there is a pure bending zone, in which the relative slip between concrete and steel mesh laminate is very small, resulting in a low level of interfacial stress. However, the slip increases when approaching the support. Therefore, the area, referred to as the 'effective area', outside the pure bending zone, mainly contributes to the capacity of the composite section. For specimens with smaller L_s,

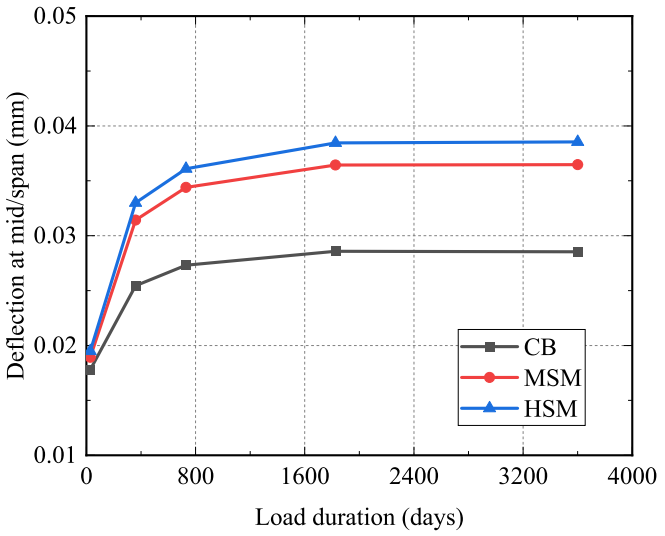

Fig. 23. Deflection at mid-span with increasing load duration.

the effective area would be reduced accordingly and hence affecting reducing the bearing capacity of the beam.

5.3. *Effect of concrete creep and shrinkage*

Concrete creep could cause significant problems for structural elements subjected to durable loads. However, in this study, the effect of concrete creep and shrinkage only dominated during the period the specimens were preserved in the laboratory before testing. Thus, the mechanical response of a simply supported strengthened beam, subjected to self-weight only, was investigated.

Fig. 23 compares the mid-span deflection of an unstrengthened beam with two GSM strengthened beams at loading durations of 28, 360, 730, 1825 and 3650 days. After 5 years of the action of the gravity, the mid-span deflection of MSM strengthened beam remained at a stable level, which was around 1.93 times of the initial deflection (1.6 times for control beam and 1.98 times for HSM strengthened beam). In addition, it can be observed that the GSM strengthened beam deflected more than the control beam, which indicates that the strengthening material could not prevent the development of deflection caused by concrete creep and shrinkage.

6. Conclusions

An experimental and numerical study on the durability performance of reinforced concrete (RC) beams strengthened by galvanized steel mesh (GSM) epoxy systems was presented in this paper. In addition, three-dimensional finite analysis model was developed to simulate the mechanical response of the tested specimens. Based on the results from this study, the following conclusions are made:

(1) The experimental results showed an improvement ranging from 46% ~ 57% in the ultimate attained load of GSM strengthened beams, with an initial cracking load 33% ~ 35% higher in comparison to the unstrengthened control beam specimens.
(2) The failure mode changed from the typical bending failure (control beam) to the delamination of concrete cover at the ends of the GSM laminate (GSM strengthened beam).
(3) While time-dependent effect of the concrete has limited influence on the initial cracking load of RC beams before and after strengthening, the ultimate load increased gradually with loading time due to concrete strength development with time. Based on the parametric study of FE simulations considering concrete creep and shrinkage, the deflections of both control and GSM strengthened beams remained stable after 5 years, and the presence of GSM strengthening materials did not prevent the development of deflection caused by concrete creep and shrinkage.
(4) Excluding any pre-loading effects, both load-deflection responses and strain development predicted by the finite element models showed good agreement with the experimental results, proving the reliability of the proposed model.
(5) Conducting a parametric study with the numerical simulations, the effects of interfacial bond strength, local debonding and the dimensions of steel mesh laminate were investigated. The results showed that the yield load and corresponding deflection decreased gradually with the decrease of interfacial bond strength. The location of local debonding barely had an effect on the load bearing capacity of the GSM strengthened beam. The dimensions of the GSM showed that decreasing the width of the GSM laminate reduced the yield and ultimate loads of the beam. In addition, it was observed that there was an increase in beam capacity with increasing the length of GSM laminate until it reached 80% of its length.

CRediT authorship contribution statement

Rui Hao: Writing – original draft, Formal analysis, Validation, Software. **Weiwei Lin:** Writing – review & editing, Formal analysis, Validation, Supervision. **Nasser A. Al-Nuaimi:** Conceptualization, Funding acquisition, Supervision, Writing – review & editing, Data curation. **Rami A. Hawileh:** Funding acquisition, Supervision, Writing – review & editing. **Jamal A. Abdalla:** Funding acquisition, Supervision. **Mohammed Z.E.B. Elshafie:** Conceptualization, Formal analysis, Validation, Writing – review & editing, Supervision.

Declaration of Competing Interest

The authors declare that they have no known competing financial interests or personal relationships that could have appeared to influence the work reported in this paper.

Acknowledgement

The funding for this research was provided by the National Priorities Research Program of the Qatar National Research Fund (A member of the Qatar Foundation) under the award no. NPRP 8-418-2-175. The statements made herein are solely the responsibility of the authors and do not necessarily reflect the opinions of the research sponsor. The authors would like to also thank Dr. Paolo Casadei from Kerakoll Spa for providing and installing the galvanized steel mesh sheets.

References

[1] M.Z. Naser, R.A. Hawileh, J.A. Abdalla, Fiber-reinforced polymer composites in strengthening reinforced concrete structures: A critical review, Eng. Struct. 198 (2019) 109542, https://doi.org/10.1016/j.engstruct.2019.109542.
[2] G. Arslan, F. Sevuk, I. Ekiz, Steel plate contribution to load-carrying capacity of retrofitted RC beams, Constr. Build. Mater. 22 (3) (2008) 143–153, https://doi.org/10.1016/j.conbuildmat.2006.10.009.
[3] A.S.D. Salama, R.A. Hawileh, J.A. Abdalla, Performance of externally strengthened RC beams with side-bonded CFRP sheets, Compos. Struct. 212 (2019) 281–290, https://doi.org/10.1016/j.compstruct.2019.01.045.
[4] D.M.V. Faria, V.J.G. Lúcio, A.P. Ramos, Strengthening of flat slabs with post-tensioning using anchorages by bonding, Eng. Struct. 33 (6) (2011) 2025–2043, https://doi.org/10.1016/j.engstruct.2011.02.039.
[5] T. Siwowski, B. Piątek, P. Siwowska, A. Wiater, Development and implementation of CFRP post-tensioning system for bridge strengthening, Eng. Struct. 207 (2020) 110266, https://doi.org/10.1016/j.engstruct.2020.110266.
[6] K.G. Vandoros, S.E. Dritsos, Concrete jacket construction detail effectiveness when strengthening RC columns, Constr. Build. Mater. 22 (3) (2008) 264–276, https://doi.org/10.1016/j.conbuildmat.2006.08.019.
[7] X. Zhang, Y. Luo, L. Wang, J. Zhang, W. Wu, C. Yang, Flexural strengthening of damaged RC T-beams using self-compacting concrete jacketing under different sustaining load, Constr. Build. Mater. 172 (2018) 185–195, https://doi.org/10.1016/j.conbuildmat.2018.03.245.

[8] A. Siddikaa, M.A. Al Mamunb, W. Ferdousc, et, al., Performances, challenges and opportunities in strengthening reinforced concrete structures by using FRPs – A state-of-the-art review, Eng. Fail Anal. 111 (2020) 104480. https://doi.org/10.1016/j.engfailanal.2020.104480.
[9] M. Ekenel, J.J. Myers, Durability performance of RC beams strengthened with epoxy injection and CFRP fabrics, Constr. Build. Mater. 21 (6) (2007) 1182–1190, https://doi.org/10.1016/j.conbuildmat.2006.06.020.
[10] G. Xing, T. Wu, B. Liu, H. Huang, S. Gu, Experimental investigation of reinforced concrete T-beams strengthened with steel wire mesh embedded in polymer mortar overlay, Adv. Struct. Eng. 13 (1) (2010) 69–79, https://doi.org/10.1260/1369-4332.13.1.69.
[11] A. Napoli, R. Realfonzo, Reinforced concrete beams strengthened with SRP/SRG systems: Experimental investigation, Constr. Build. Mater. 93 (2015) 654–677, https://doi.org/10.1016/j.conbuildmat.2015.06.027.
[12] R.A. Hawileh, W. Nawaz, J.A. Abdalla, Flexural behavior of reinforced concrete beams externally strengthened with Hardwire Steel-Fibers, Constr. Build. Mater. 172 (2018) 562–573, https://doi.org/10.1016/j.conbuildmat.2018.03.225.
[13] A.A.M. Mohamed, A.T. Bassam, M.Z. Mohamed, Flexural behavior of RC beams strengthened with steel wire mesh and self-compacting concrete jacketing - Experimental investigation and test results, J. Mater. Res. Technol. 10 (2021) 1002–1019, https://doi.org/10.1016/j.jmrt.2020.12.069.
[14] J.A. Abdalla, A. Mohammmed, R.A. Hawileh, Flexural Strengthening of Reinforced Concrete Beams with Externally Bonded Hybrid Systems, Proc. Struct. Integr. 28 (2020) 2312–2319, https://doi.org/10.1016/j.prostr.2020.11.078.
[15] F. Yuan, M. Chen, J. Pan, Flexural strengthening of reinforced concrete beams with high-strength steel wire and engineered cementitious composites, Constr. Build. Mater. 254 (2020) 119284, https://doi.org/10.1016/j.conbuildmat.2020.119284.
[16] N. Al Nuaimi, M.G. Sohail, R.A. Hawileh, J.A. Abdalla, K. Douier, Durability of reinforced concrete beams strengthened by galvanized steel mesh-epoxy systems under harsh environmental conditions, Compos. Struct. 249 (2020) 112547, https://doi.org/10.1016/j.compstruct.2020.112547.
[17] A.F. Al-Khafaji, J.J. Myers, W. Wang, Bond evaluation of SRP strengthening system exposed to several harsh environmental conditions, Constr. Build. Mater. 231 (2020) 117093, https://doi.org/10.1016/j.conbuildmat.2019.117093.
[18] M. Hasani, F. Moghadas Nejad, J. Sobhani, M. Chini, Mechanical and durability properties of fiber reinforced concrete overlay: Experimental results and numerical simulation, Constr. Build. Mater. 268 (2021) 121083, https://doi.org/10.1016/j.conbuildmat.2020.121083.
[19] A. Godat, P. Labossière, K.W. Neale, Numerical investigation of the parameters influencing the behaviour of FRP shear-strengthened beams, Constr. Build. Mater. 32 (2012) 90–98, https://doi.org/10.1016/j.conbuildmat.2010.11.110.
[20] Y.T. Obaidat, S. Heyden, O. Dahlblom, The effect of CFRP and CFRP/concrete interface models when modelling retrofitted RC beams with FEM, Compos. Struct. 92 (6) (2010) 1391–1398, https://doi.org/10.1016/j.compstruct.2009.11.008.
[21] Y.T. Obaidat, S. Heyden, O. Dahlblom, Evaluation of parameters of bond action between FRP and concrete, J. Compos. Constr. 17 (5) (2013) 626–635, https://doi.org/10.1061/(ASCE)CC.1943-5614.0000378.
[22] X. Wang, C. Zhou, J. Ai, M. Petrů, Y. Liu, Numerical investigation for the fatigue performance of reinforced concrete beams strengthened with external prestressed HFRP sheet, Constr. Build. Mater. 237 (2020) 117601, https://doi.org/10.1016/j.conbuildmat.2019.117601.
[23] M.M.A. Kadhim, A.R. Jawdhari, M.J. Altaee, A.H. Adheem, Finite element modelling and parametric analysis of FRP strengthened RC beams under impact load, J. Build. Eng. 32 (2020) 101526, https://doi.org/10.1016/j.jobe.2020.101526.
[24] F. Ascione, M. Lamberti, A. Napoli, A.G. Razaqpur, R. Realfonzo, Modeling SRP-concrete interfacial bond behavior and strength, Eng. Struct. 187 (2019) 220–230, https://doi.org/10.1016/j.engstruct.2019.02.050.
[25] F. Ascione, M. Lamberti, A. Napoli, G. Razaqpur, R. Realfonzo, An experimental investigation on the bond behavior of steel reinforced polymers on concrete substrate, Compos. Struct. 181 (2017) 58–72, https://doi.org/10.1016/j.compstruct.2017.08.063.
[26] X.Z. Lu, J.G. Teng, L.P. Ye, J.J. Jiang, Bond-slip models for FRP sheets/plates bonded to concrete, Eng. Struct. 27 (6) (2005) 920–937, https://doi.org/10.1016/j.engstruct.2005.01.014.
[27] F. Bencardino, A. Condello, SRG/SRP–concrete bond–slip laws for externally strengthened RC beams, Compos. Struct. 132 (2015) 804–815, https://doi.org/10.1016/j.compstruct.2015.06.068.
[28] JSCE, Standard Specification for Concrete Structures, Tokyo, Japan, 2007.
[29] CEB-FIP. fib Model Code for Concrete Structures, Lausanne, Switzerland, 2010.
[30] ACI committee 440., Guide for the design and construction of externally bonded FRP systems for strengthening concrete structures (ACI 440. 2R-17). American Concrete Institute 2017, Farmington Hills, Mich.